Nonlinear Dynamics (2026) 114:405
https://doi.org/10.1007/s11071-026-12277-2

RESEARCH

Escape from a coupled bi-quartic potential well

Attila Genda[1] · Alexander Fidlin[1] · Oleg V. Gendelman[2]

Received: 27 February 2025 / Revised: 24 November 2025 / Accepted: 14 January 2026

Abstract

In this paper, we investigate the dynamics of particles within a bi-quartic potential well, characterized by the coupled potential function $V(x, y) = \frac{1}{2}x^2 + \frac{1}{2}y^2 - \frac{1}{4}x^4 - \frac{1}{4}y^4 + Cx^2y^2$. Our focus is on the safe basins of escape and level-crossing under arbitrary initial conditions, i.e., the spatial region of initial conditions from where an initiated motion of the particle remains bounded. The coupling term allows energy exchange between the modes. If the total energy is sufficient, a particle starting from a given set of initial conditions within the potential well can reach the escape boundary over time, which would not occur without coupling. We find that escape trajectories often pass near one of the four saddles of the potential. Numerical simulations reveal that the safe basins of escape have fractal boundaries due to the energy-exchange mechanism. To address safety-critical applications where these chaotic regimes must be avoided, we introduce a factor of safety that defines a safety region. Crossing the safety region's boundary shifts the problem from escape to level-crossing. Assuming harmonic-like solutions of the differential equations with slowly varying amplitudes and phases, we transform our system into an appropriate form for averaging. By eliminating time as a variable and realizing that only the phase difference is significant, we derive two first integrals of the particle motion in analytic form, which allows us to analytically determine the safe region boundary and calculate its size based on the coupling parameter C.

Keywords Safe basins · Potential well · Coupled oscillator · Initial conditions · Escape · Level-crossing

1 Introduction

Many physical and engineering systems exhibit transitions across a critical boundary, often treated as the *problem of escape from a potential well*. Examples include molecular dynamics of adsorbed particles [1, 2], gravitational collapse in celestial mechanics [3, 4], energy harvesting [5], Josephson junctions [6], ship-capsizing [7, 8], biological systems [9] and dynamic pull-in instabilities in microelectromechanical systems (MEMS) [10–12]. Traditional studies of such systems frequently address complete escape – that is, trajectories passing entirely over a potential barrier. However, in many applications, it suffices to examine whether the system crosses a predefined threshold (the end of a safety region) rather than escaping altogether, which we call a *level-crossing problem* [13–20].

Early analyses of escape-type phenomena showed that external forcing can significantly affect the transition across potential barriers [13, 21], with methods such as harmonic balance and bifurcation analysis proving useful. Other works used different analytical approaches, including canonical transformations for isolated resonances [16, 17, 22] and multi-degree-of-freedom (MDOF) extensions [23, 24]. Under certain forcing laws, fractal boundaries separate escaping trajectories from non-escaping ones, highlighting extreme sensitivity to initial conditions (ICs) [25–27]. Such sensitivity can become even more pronounced in the presence of noise [28, 29], where fluctuations lead to chaotic scattering and fractal escape basins.

Accurate prediction of whether trajectories cross a given boundary is essential for safe design and optimization in numerous contexts [30, 31]. In the simpler one-degree-of-freedom (1DOF) setting, analytical methods such as multiple

✉ Attila Genda
attila.genda@kit.edu

Alexander Fidlin
alexander.fidlin@kit.edu

Oleg V. Gendelman
ovgend@me.technion.ac.il

[1] Institute of Engineering Mechanics, Karlsruhe Institute of Technology, Kaiserstr. 12, 76131 Karlsruhe, Germany

[2] Faculty of Mechanical Engineering, Technion - Israel Institute of Technology, Haifa 3200003, Israel

Published online: 16 March 2026

scales and the Melnikov criterion have been deployed to estimate escape conditions [32, 33]. Nevertheless, for many practical problems, one does not require the complete analysis of unbounded motion but rather the location and timing of the level crossing itself.

The concept of safe basins (SBs), also referred to as basins of attraction or catchment regions, has proven indispensable for assessing whether solutions remain within a stable region under excitation, parameter variations, or uncertain ICs [21, 34]. Determining the exact shape and size (global integrity measure (GIM)) of an SB is a computationally highly intensive task [35], which is also mostly pointless from a practical point of view since such basins often have fractal-like boundaries, where escaping and non-escaping solutions lie in an infinitesimal vicinity of each other. To not refer to such regions as safe, various local integrity measures have been developed [36], and several numerical algorithms have been developed to assess such basins [34, 35, 37, 38]. Nevertheless, most works on assessing an integrity measure for dynamical systems are performed numerically, and only a few papers have reported analytical computations of SBs [19, 20, 39–41], limited to two-dimensional phase space.

In this work, we consider the same 2DOF oscillator as explored in [41], but in a somewhat extended version. In our investigation, we allow for arbitrary ICs and seek the equation of the SB boundary in the complete four-dimensional IC space. Instead of employing the canonical action–angle framework [16, 17, 22, 42], we adopt an averaging approach that presumes a 1:1 resonance, seeking a more direct analysis of the level crossing. The primary goal is to understand how ICs determine whether the boundary of the safe region is reached. After averaging, the number of variables can be reduced by one, since only the phase difference of the averaged equations is required. Energy conservation in the averaged system further reduces the number of variables by one, and subsequent elimination of time yields an ODE that can be solved analytically in closed form. The solution is an additional conservation law, only present in the averaged system [42]. With the help of the analytical solution, a polynomial expression is provided to describe the four-dimensional SB boundary. It should be emphasized that this additional conserved quantity is not a new finding of the present work. Its existence for general two-degree-of-freedom conservative systems with weak nonlinear coupling has been known since the classical studies of *Gilchrist* [43], *Kronauer et al.* [44], and *Musa* [45], who derived this invariant in a general form including second- and third-order coupling terms. Moreover, the additional conserved quantity also exists for large nonlinearities, as shown by [42, 46, 47]. Our current system is a special case of *Gilchrist*'s general formulation with $m_1 = p_1 = m_2 = p_2 = 0$.

The novelty of the present work lies in applying this established invariant to derive and quantify safe basins in coupled oscillators, a topic not addressed in the classical literature.

The paper is structured as follows. In Sect. 2, the problem setting is presented, and definitions of escape and level-crossing are formulated in mathematical terms. Section 3 reduces the system to the slow manifold using averaging, and the solution of the slow system is then found analytically. In Sect. 4, the volume of the safe basin is calculated as a function of the coupling parameter C. In Sect. 5, the analytical results are compared to numerical Monte Carlo simulations. Section 6 summarizes the findings and outlines potential directions for future research.

2 Problem setting

We investigate the escape problem of a particle of unit mass in the two-dimensional potential

$$V(x, y) = \frac{x^2}{2} - \frac{x^4}{4} + \frac{y^2}{2} - \frac{y^4}{4} - Cx^2y^2, \tag{1}$$

where $C \in [0, 0.5]$ is the coupling parameter (cf. Fig. 1). The following nonlinear differential equation system gives the equations of motion:

$$\ddot{x} + x - x^3 - 2Cxy^2 = 0, \tag{2}$$
$$\ddot{y} + y - y^3 - 2Cx^2y = 0, \tag{3}$$
$$x(0) = x_0, \quad \dot{x}(0) = u_0, \tag{4}$$
$$y(0) = y_0, \quad \dot{y}(0) = v_0. \tag{5}$$

We denote the solution of the equations by

$$\mathbf{f}(t, \mathbf{x_0}) = \begin{pmatrix} x(t, \mathbf{x_0}) \\ y(t, \mathbf{x_0}) \end{pmatrix}. \tag{6}$$

In Figs. 2, 3, 4, 5, different trajectories are shown.

Before starting the analysis, we have to define some of the terms we are dealing with. When referring to *escape*, one expects a motion starting from the *interior* of a potential well and leading to the *outside* of the well. A *potential well* is well-defined in terms of the position coordinates; we can think of a definition equivalent to a *drainage basin* in geology.

Definition 1 (Drainage basin for the potential V) Let $V : \mathbb{R}^2 \to \mathbb{R}$ be C^2 with locally Lipschitz gradient. Consider the first-order downhill gradient flow

$$\dot{\mathbf{z}}(t) = -\nabla V(\mathbf{z}(t)), \qquad \mathbf{z}(t) = (x(t), y(t)) \in \mathbb{R}^2. \tag{7}$$

For $\mathbf{z}_0 \in \mathbb{R}^2$ let $\psi(t; \mathbf{z}_0)$ denote the unique solution with $\psi(0; \mathbf{z}_0) = \mathbf{z}_0$. Let $\mathcal{M} = \{m_k\}$ be the set of isolated,

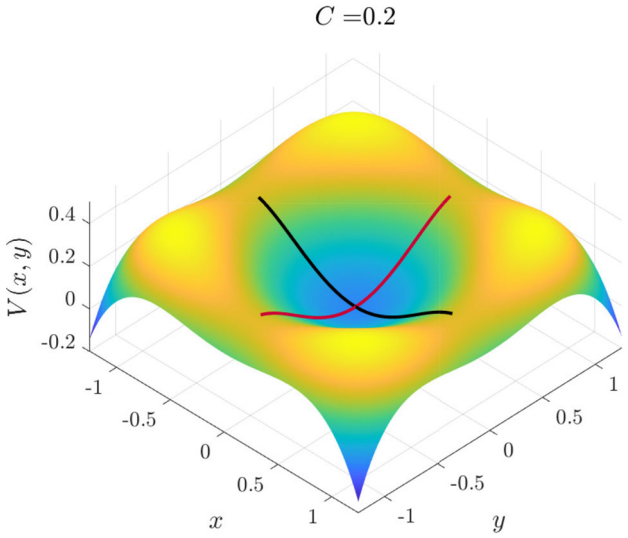

Fig. 1 Potential function with solutions along the coordinate axis

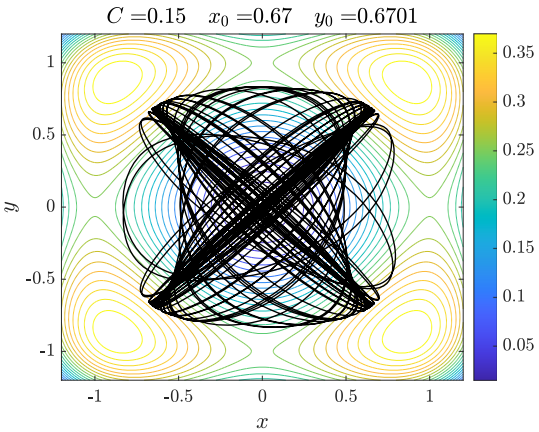

Fig. 2 Unstable diagonal oscillations

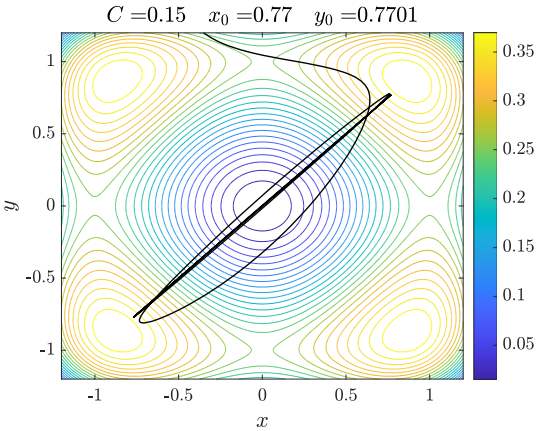

Fig. 3 Escape through the vicinity of a saddle point

nondegenerate local minima of V. The *drainage basin* of a minimum m_k is the set

$$\mathcal{B}(m_k) = \left\{ \mathbf{z}_0 \in \mathbb{R}^2 : \lim_{t\to\infty} \psi(t; \mathbf{z}_0) = m_k \right\}. \tag{8}$$

That is, $\mathcal{B}(m_k)$ collects exactly those initial positions from which the downhill flow converges to m_k.

Definition 2 (Watershed of V) Let $\{s_j\}$ be the index-1 saddle points of V. The *watershed* Γ is the union of the separatrices that separate the drainage basins. It is characterized by

$$\Gamma = \bigcup_j W^s_{\nabla V}(s_j), \tag{9}$$

where

$$W^s_{\nabla V}(s_j) = \left\{ \mathbf{z}_0 \in \mathbb{R}^2 : \lim_{t\to+\infty} \psi(t; \mathbf{z}_0) = s_j \right\}, \tag{10}$$

Remark 1 For the quartic potential in (2) with $C \in [0, 0.5)$, the four nontrivial maxima occur at $m_{(\sigma_x,\sigma_y)} = (\sigma_x a, \sigma_y a)$ with $a = (1 + 2C)^{-1/2}$ and $\sigma_x, \sigma_y \in \{\pm 1\}$. The four points $(\pm 1, 0)$ and $(0, \pm 1)$ are index-1 saddles (for $C < \frac{1}{2}$; a degeneracy appears at $C = \frac{1}{2}$). The watershed Γ is formed by the separatrices emanating from the maxima towards the saddles under the downhill flow and partitions $\mathbb{R}^2$ into the drainage basin of the local minimum at the origin and the rest of the plane diverging to infinity. For a visual representation, see Fig. 6.

However, in the drainage basin case, inertia is neglected, whereas in our study, it plays a crucial role in the dynamics. Thus, the velocity coordinates are also included in the analysis, yielding a four-dimensional phase space in which the meaning of a potential well becomes ambiguous. As a consequence, the definition of an *escape event* is also unclear in a four-dimensional setting. However, we can still find a clear distinction between two sets of ICs when looking at the long-term behavior of the corresponding trajectories: a set with a bounded trajectory and a set with an unbounded trajectory as time approaches infinity.

Definition 3 (Safe Basin of Escape (SBOE) and Unbounded Set (US)) For System (2)-(3), an IC $\mathbf{x}_0$ is called *safe* if the corresponding solution remains bounded for all time, i.e.:

$$||\mathbf{f}(t, \mathbf{x_0})|| < \infty \quad \text{as } t \to \infty. \tag{11}$$

The set of all ICs $\mathbf{x_0} \in \mathbb{R}^4$ leading to bounded solutions is called the *safe basin of escape* (SBOE). All other initial conditions belong to the *unbounded set* (US).

Remark 2 Since we are interested in SBs with non-zero measures, we will not go into details regarding the treatment of

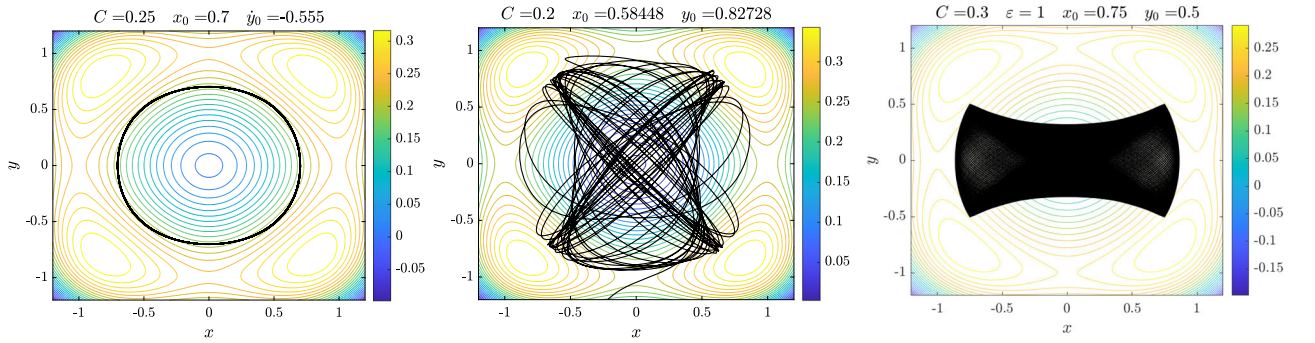

(a) Almost circular orbit **(b)** Chaotic escape through the vicinity of a saddle point **(c)** Quasi-periodic oscillations within well-defined boundaries

Fig. 4 Different kinds of solutions in the vicinity of the 1:1 manifold. The colored lines correspond to different energy levels of $V(x, y)$

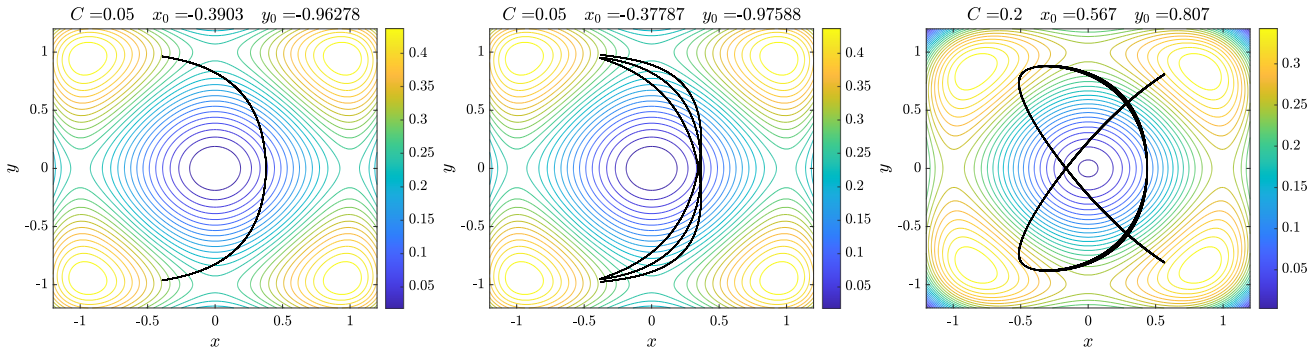

(a) Stable 2:1 oscillation **(b)** Subharmonic 2:1 oscillation **(c)** Stable 4:3 oscillation

Fig. 5 Different kinds of stable but non-1:1 oscillations. The colored lines correspond to different energy levels of $V(x, y)$

such sets of points that fulfill Def. 3 but are commonly not referred to as SB due to their zero volume. Such zero-volume sets consist of ICs with trajectories converging to one of the system's unstable fixed points.

Observations show that for $C \neq 0$ unbounded trajectories starting near the boundary of the SBOE exit the potential well near the four saddle points located at $(\pm 1, 0)$ and $(0, \pm 1)$. We focus on the maximum displacements observed along any of the axes to provide a more precise characterization of escape. With

$$d(t) := \max\{|x(t)|, |y(t)|\}, \tag{12}$$

we define

$$d_{\max}(T) := \max_{t\in[0,T]} d(t). \tag{13}$$

Thus, an escape occurs if and only if $\exists\, T \in \mathbb{R}_0^+$ such that $d(T) > 1$ (except the cases described in Remark 2). This formulation is much more practical since, in case a trajectory is unbounded, the solution does not have to be calculated for all times, just until the occurrence of the event $d(T_{\text{esc}}) =$

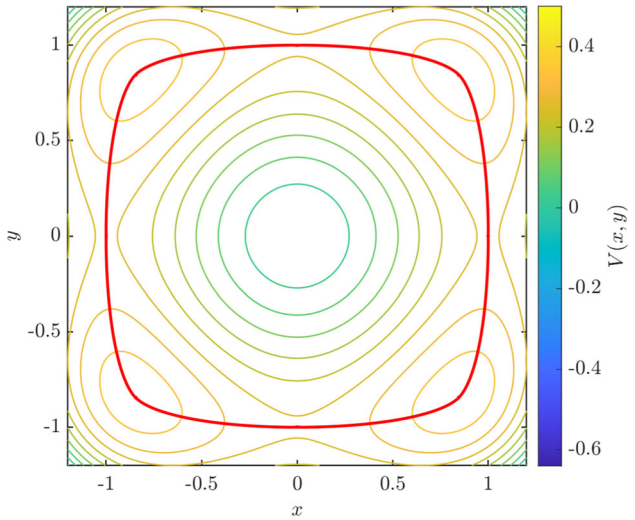

$C = 0.20$

Fig. 6 Contour plot of $V(x, y)$ with watershed (red) for $C = 0.2$. An animated version of this figure is available in the Electronic Supplementary Material (`animated_watershed.mp4`)

1 (in the following, we will call this an *escape event*). By this condition, the somewhat ambiguous escape problem is reformulated as an unambiguous level-crossing problem, and the SBOE can also be redefined as follows.

Definition 4 (Safe Basin of Level Crossing (SBOLC))

$$SBOLC(L) := \{\mathbf{x_0} \in \mathbb{R}^4 \mid d_{\max}(T) < L \; \forall \; T \geq 0\}. \quad (14)$$

For the above-mentioned case, $L = 1$.

It is easy to see by Liouville's theorem that the projection of the SBOLC on the $x - y$ plane (except for the cases described in Remark 2) cannot reach beyond the square $[-1, 1] \times [-1, 1]$ since that would mean that a trajectory enters the well from outside and remains in it forever. Since the system is conservative, the same trajectory also belongs to a point moving in reverse time; being a non-escaping trajectory, it can never leave the square. Thus, we have a contradiction.

Engel et al. observed in [41] that the boundary of the SB is fractal-like even in the case of zero-velocity ICs, an indicator of chaotic behavior. In real-life scenarios and engineering applications, chaotic behavior is usually considered unsafe, even if escape does not occur during the simulation. The latter is necessarily finite and cannot provide reliable information about behavior over a longer time span. It is common to introduce safety factors to account for uncertainties in such cases.

Definition 5 (Safety factor and safe region (*SF* and *SR*)) For a given *safety factor* $SF > 1$, the corresponding *safe region* $SR \subset \mathbb{R}^2$ is defined as

$$SR := \left\{ (x, y) \in \mathbb{R}^2 \;\middle|\; x \in \left[-\tfrac{1}{SF}, \tfrac{1}{SF}\right], \; y \in \left[-\tfrac{1}{SF}, \tfrac{1}{SF}\right] \right\}. \quad (15)$$

For a graphical representation of the SR, see Fig. 7a .
For the sake of the formal analysis, we introduce a large SF to investigate the level-crossing problem with $\sqrt{\varepsilon} := L = 1/SF$, where ε is a small, but not precisely defined, positive real number. Later, we will also assess the analytical results for practically relevant small values of the safety factor, for which the underlying assumptions are formally violated, and compare them with numerical results. By introducing the non-dimensional variables

$$X := \frac{x}{\sqrt{\varepsilon}}, \qquad Y := \frac{y}{\sqrt{\varepsilon}}, \quad (16)$$

we can write the modified potential

$$V_\varepsilon(X, Y) = \frac{X^2}{2} + \frac{Y^2}{2} - \varepsilon\left(\frac{X^4}{4} + \frac{Y^4}{4} + CX^2Y^2\right), \quad (17)$$

and the non-dimensional system of differential equations

$$\ddot{X} + X - \varepsilon X^3 - 2\varepsilon C X Y^2 = 0, \quad (18)$$
$$\ddot{Y} + Y - \varepsilon Y^3 - 2\varepsilon C X^2 Y = 0, \quad (19)$$
$$X(0) = X_0, \quad Y(0) = Y_0, \quad (20)$$
$$\dot{X}(0) = \frac{u_0}{\sqrt{\varepsilon}} =: U_0, \quad \dot{Y}(0) = \frac{v_0}{\sqrt{\varepsilon}} =: V_0. \quad (21)$$

3 Reduction to the 1:1 slow manifold

In the following, the system is transformed to slow-variables, $A_x(\tau)$, $A_y(\tau)$, $\Psi_x(\tau)$ and $\Psi_y(\tau)$, with $\tau := \varepsilon t$ and the corresponding derivative $\square' = \mathrm{d}\square/\mathrm{d}\tau$. We assume that the motion takes the form

$$X(t) = A_x(\tau)\sin(t + \Psi_x(\tau)),$$
$$\dot{X}(t) = A_x(\tau)\cos(t + \Psi_x(\tau)), \quad (22)$$
$$Y(t) = A_y(\tau)\sin(t + \Psi_y(\tau)),$$
$$\dot{Y}(t) = A_y(\tau)\cos(t + \Psi_y(\tau)). \quad (23)$$

These assumptions are natural, since system (18)-(19) is linear at $\mathcal{O}(1)$, admitting harmonic oscillations as solutions. Nonlinearities and energy exchange are only present at $\mathcal{O}(\varepsilon)$, thus, the changes of amplitude and phase shift are slow [48]. On the other hand, for the derivatives, we also have

$$\dot{X}(t) = \dot{A}_x \sin(t + \Psi_x) + A_x(1 + \dot{\Psi}_x)\cos(t + \Psi_x), \quad (24)$$
$$\dot{Y}(t) = \dot{A}_y \sin(t + \Psi_y) + A_y(1 + \dot{\Psi}_y)\cos(t + \Psi_y) \quad (25)$$

and making use of Van der Pol's transformation, we obtain

$$\dot{A}_x = \varepsilon\Big(A_x^3 \sin^3(t + \Psi_x)\cos(t + \Psi_x) + 2C A_x A_y^2 \sin(t + \Psi_x)\cos(t + \Psi_x) \sin^2(t + \Psi_y)\Big), \quad (26)$$
$$\dot{\Psi}_x = \varepsilon\Big(-A_x^2 \sin^4(t + \Psi_x) - 2C A_y^2 \sin^2(t + \Psi_x)\sin^2(t + \Psi_y)\Big), \quad (27)$$
$$\dot{A}_y = \varepsilon\Big(A_y^3 \sin^3(t + \Psi_y)\cos(t + \Psi_y) + 2C A_x^2 A_y \sin(t + \Psi_y)\cos(t + \Psi_y)\sin^2(t + \Psi_x)\Big), \quad (28)$$
$$\dot{\Psi}_y = \varepsilon\Big(-A_y^2 \sin^4(t + \Psi_y) - 2C A_x^2 \sin^2(t + \Psi_x)\sin^2(t + \Psi_y)\Big). \quad (29)$$

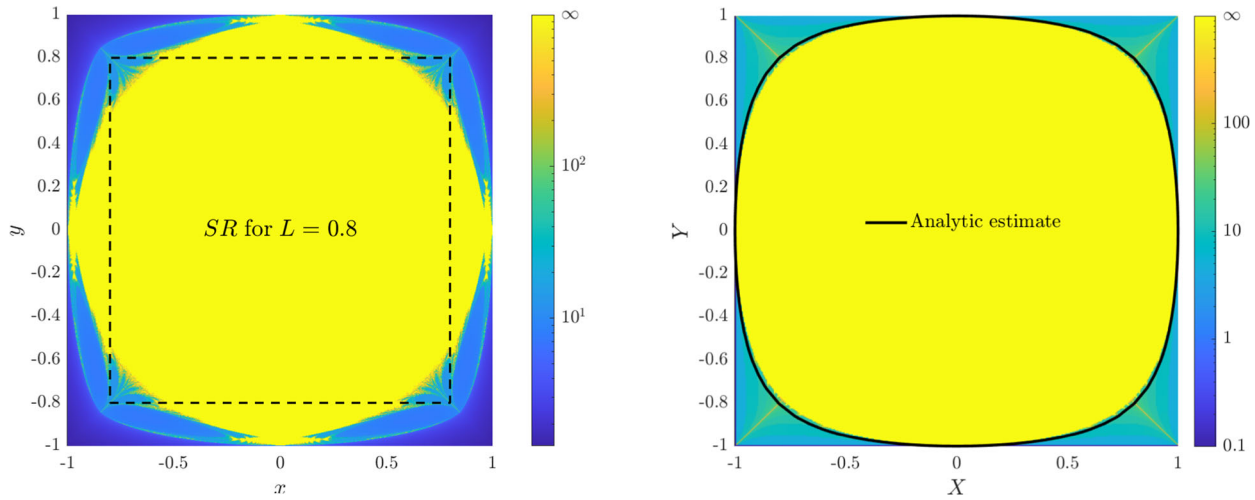

(a) SBOE (depicted with yellow) with a fractal-like boundary. The SR, used in Fig. 7b is depicted with dashed line for SF=1.25.

(b) SBOLC (depicted with yellow) with a smooth boundary. The analytical estimate (cf. Eq.(60)) shows good agreement with the numerically obtained exact solution for L=0.8, corresponding to SF=1.25.

Fig. 7 Sections of SBOE (a) and SBOLC (b) along $u_0 = v_0 = 0$ for parameter choice $C = 0.2$. The color scale represents the escape/level-crossing times of numerical solutions

After averaging the right-hand side and rewriting the equations in the slow time, we obtain

$$A_x' = -\frac{C A_x A_y^2}{4} \sin\left(2\left(\Psi_x - \Psi_y\right)\right), \tag{30}$$

$$\Psi_x' = -\frac{3}{8}A_x^2 - \frac{C}{2}A_y^2\left(1 + \frac{1}{2}\cos\left(2\left(\Psi_x - \Psi_y\right)\right)\right), \tag{31}$$

$$A_y' = -\frac{C A_x^2 A_y}{4} \sin\left(2\left(\Psi_y - \Psi_x\right)\right), \tag{32}$$

$$\Psi_y' = -\frac{3}{8}A_y^2 - \frac{C}{2}A_x^2\left(1 + \frac{1}{2}\cos\left(2\left(\Psi_y - \Psi_x\right)\right)\right). \tag{33}$$

For weakly nonlinear systems, the above averaging technique is standard, and the solution differs from the original system's solution only at ε on a time-scale of $\mathcal{O}(1/\varepsilon)$ [48]. Comparisons between the solutions of Eqs. (18)- (19) and Eqs. (30)-(33) are shown in Figs. 8- 9.

The averaged equations in the slow variables still have the same number of degrees of freedom as the original system. However, the system order can be reduced. First, we note that on the right-hand side, only the difference $\Psi_x - \Psi_y$ is present. Thus, by subtracting Eq. (33) from Eq. (31) we obtain the nonlinear ODE system

$$A_x' = -\frac{C A_x A_y^2}{4} \sin\left(2\Delta_\Psi\right), \tag{34}$$

$$A_y' = \frac{C A_x^2 A_y}{4} \sin\left(2\Delta_\Psi\right), \tag{35}$$

$$\Delta_\Psi' = \frac{A_x^2 - A_y^2}{2}\left(-\frac{3}{4} + C\left(1 + \frac{1}{2}\cos(2\Delta_\Psi)\right)\right). \tag{36}$$

It is easy to find fixed points and partially stationary solutions of Eqs. (30)-(33). Note that the equilibrium position at $(x_0, y_0) = (0, 0)$ corresponding to $A_x = A_y = \Psi_x = \Psi_y = 0$ is also a solution of the averaged system. Periodic solutions of Eq. (2)-(3) are obtained if $\dot{A}_x = \dot{A}_y = 0$ and $\dot{\Psi}_x - \dot{\Psi}_y = 0$, but $\dot{\Psi}_x \neq$ and $\dot{\Psi}_y \neq 0$. Fixed points are given for:

- Stable circular orbits (cf. Fig. 4a): $A_x = A_y = A_0 > 0$ and $\Psi_1 = \Psi_2 + k\pi/2$ with $k \in \{1, 3\}$,
- Unstable 1 DOF Oscillations along the diagonals (cf. Fig. 2): $A_x = A_y = A_0 > 0$ and $\Psi_1 = \Psi_2 + k\pi/2$ with $k \in \{0, 2\}$,

and partially stationary solutions are given for

- Stable 1 DOF oscillations along the coordinate axis (cf. Fig. 1): $A_y = 0$ and $A_x = A_0$ for any $0 < |A_0| < 1$ or $A_x = 0$ and $A_y = A_0$ for any $0 < |A_y| < 1$.

In the latter case, the phase difference changes with time. However, it does not influence the amplitudes, which remain constant. This behavior follows from the fact that along these axis-aligned motions, one coordinate is identically zero, which makes the coupling term vanish. Since no energy exchange between the modes is possible in this case, the phase evolution in the zero-amplitude direction does not

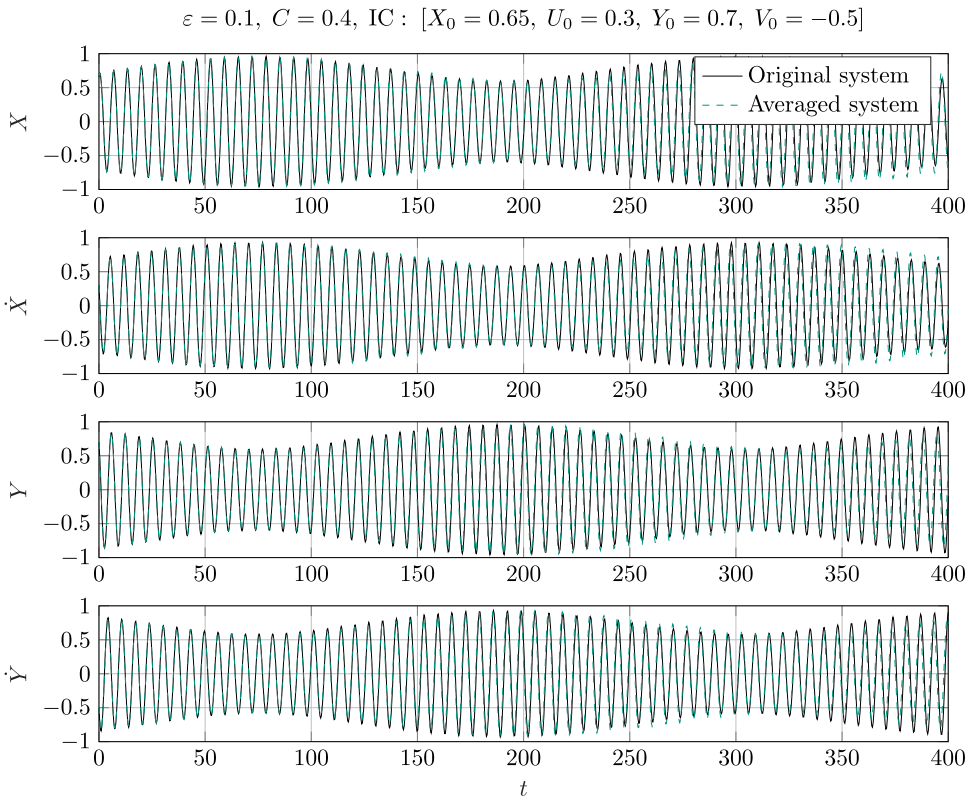

Fig. 8 Symmetric energy exchange: Comparison of the numerical solutions of the original system (18)-(19) to the averaged system (30)-(33). The averaged system effectively captures the energy exchange between modes. Errors between the original model and its averaged approximate accumulate much slower than the theoretically proven worst case rate $\mathcal{O}(1/\varepsilon)$

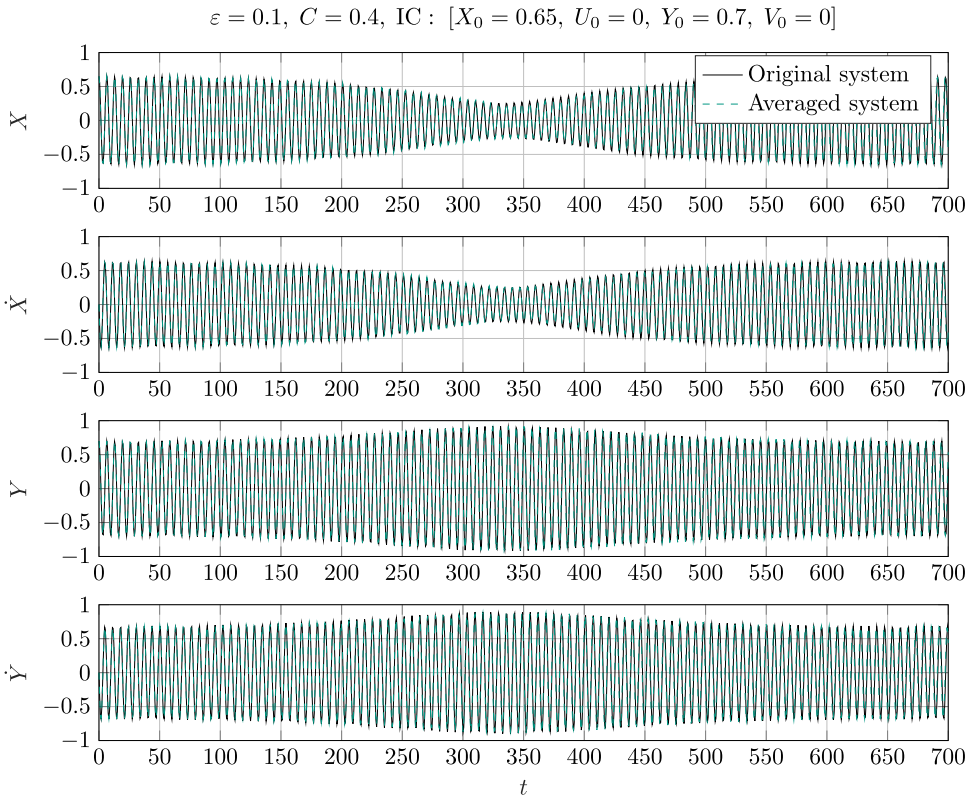

Fig. 9 Asymmetric energy exchange: Comparison of the numerical solutions of the original system (18)-(19) to the averaged system (30)-(33). The averaged system effectively captures the energy exchange between modes. Errors between the original model and its averaged approximate accumulate much slower than the theoretically proven worst case rate $\mathcal{O}(1/\varepsilon)$

affect the amplitudes. It is therefore irrelevant for the escape or level-crossing behavior.

For a stability analysis of the above solutions, see the Appendix.

3.1 General solution

To solve the differential equation, it is necessary to eliminate additional variables. Since the system is conservative, we can use the conservation of total energy, which also holds for the averaged system.

$$(A_x^2)' = 2A_x A_x' \quad \Rightarrow \quad A_x' = \frac{(A_x^2)'}{2A_x} = -\frac{C}{4} A_x A_y^2 \sin(2\Delta\Psi) \tag{37}$$

$$(A_y^2)' = 2A_y A_y' \quad \Rightarrow \quad A_y' = \frac{(A_y^2)'}{2A_y} = \frac{C}{4} A_x^2 A_y \sin(2\Delta\Psi) \tag{38}$$

which implies

$$\begin{aligned} \frac{\mathrm{d}(A_x^2 + A_y^2)}{\mathrm{d}t} = 0 \Rightarrow A_x^2 + A_y^2 &= \text{const.} \\ =: A_0^2 &= A_{x0}^2 + A_{y0}^2. \end{aligned} \tag{39}$$

Thus, we can substitute $A_x = \sqrt{A_0^2 - A_y^2}$ in Eqs. (32)–(36) and the remaining two differential equations are as follows:

$$\frac{\mathrm{d}A_y}{\mathrm{d}\tau} = \frac{C}{4} A_y (A_0^2 - A_y^2) \sin(2\Delta\Psi) \tag{40}$$

$$\frac{\mathrm{d}\Delta\Psi}{\mathrm{d}\tau} = \frac{A_0^2 - 2A_y^2}{2} \left(C - \frac{3}{4} + \frac{C}{2} \cos(2\Delta\Psi) \right). \tag{41}$$

Now, we can eliminate the time by dividing Eq. (40) by Eq. (41). We obtain

$$\frac{\mathrm{d}A_y}{\mathrm{d}\Delta\Psi} = \frac{C A_y (A_0^2 - A_y^2) \sin(2\Delta\Psi)}{2(A_0^2 - 2A_y^2) \left(C - \frac{3}{4} + \frac{C}{2} \cos(2\Delta\Psi) \right)}. \tag{42}$$

Rearranging Eq. (42) we have

$$\underbrace{2(A_0^2 - 2A_y^2) \left(C - \frac{3}{4} + \frac{C}{2} \cos(2\Delta\Psi) \right)}_{=:p(A_y, \Delta\Psi)} \mathrm{d}$$

$$A_y \underbrace{- \left(C A_y (A_0^2 - A_y^2) \sin(2\Delta\Psi) \right)}_{=:q(A_y, \Delta\Psi)} \mathrm{d}\Delta\Psi = 0. \tag{43}$$

Eq. (43) is not exact since the integrability condition is not fulfilled, i.e.,

$$\frac{\partial p}{\partial \Delta\Psi} - \frac{\partial q}{\partial A_y} = C \sin(2\Delta\Psi) \left(A_y^2 - A_0^2 \right) \neq 0. \tag{44}$$

Luckily, we can find an integrating factor of the form $\mu(A_y)$ by calculating

$$\mu(A_y) = \exp\left(\int \frac{1}{q} \left(\frac{\partial p}{\partial \Delta\Psi} - \frac{\partial q}{\partial A_y} \right) \mathrm{d}A_y \right) = A_y. \tag{45}$$

After multiplication by $\mu(A_y)$, Eq. (43) becomes an exact differential equation, which we can solve by integration, and we obtain

$$\begin{aligned} \Phi(A_y, \Delta\Psi) = \left(C - \frac{3}{4} + \frac{C}{2} \cos(2\Delta\Psi) \right) \times \\ \left(A_y^2 \left(A_0^2 - A_y^2 \right) \right) = \Phi_0 = \text{const.} \end{aligned} \tag{46}$$

Remark 3 First integrals (39) and (46) are a special case of the conservation laws described in [43, 44]. Eqs. (39) and (46) can also be interpreted as a specific, first-order approximation of the corresponding nonlinear system described in [42] by assuming only weak nonlinearity. However, in [42] the choice of independent slow variables is somewhat different. In fact, one might also use polar coordinates here to describe $A_x = (A_0 \cos\gamma)/2$ and $A_y = (A_0 \sin\gamma)/2$.

The "additional" conservation law is the slow invariant that organizes inter-modal energy exchange: it fixes the partition of the total energy between the two modes together with their slow phase relation, thereby structuring the beating dynamics on the averaged time scale.

Remark 4 We can express the A_y in terms of $\Delta\Psi$. Since A_y is an amplitude, only the positive solutions are of interest:

$$A_{y,1/2} = \sqrt{\frac{A_0^2 \pm \sqrt{A_0^4 - \frac{4\Phi_0}{C - \frac{3}{4} + \frac{C}{2}\cos(2\Delta\Psi)}}}{2}}. \tag{47}$$

Then, since $A_x^2 = A_0^2 - A_y^2$, we also have

$$A_{x,1/2} = \sqrt{\frac{A_0^2 \mp \sqrt{A_0^4 - \frac{4\Phi_0}{C - \frac{3}{4} + \frac{C}{2}\cos(2\Delta\Psi)}}}{2}}. \tag{48}$$

This means that $A_{y,1} = A_{x,2}$ and $A_{y,2} = A_{x,1}$.

Remark 5 $\Phi(A_y, \Delta\Psi) = \Phi_0 \leq 0$ for $C \in [0, \frac{1}{2}]$, since $C - \frac{3}{4} + \frac{C}{2}\cos(2\Delta\Psi) \leq C - \frac{3}{4} + \frac{C}{2} = \frac{3}{2}(C - \frac{1}{2}) \leq 0$. Thus, the value of the inner square root is always less than

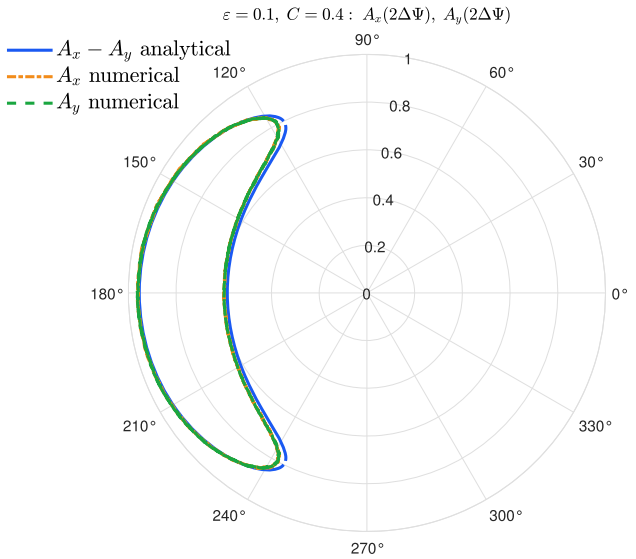

Fig. 10 Comparison of the analytical vs. numerical solution in polar coordinates for $X_0 = 0.65$, $U_0 = 0.30$, $Y_0 = 0.70$, and $V_0 = -0.50$

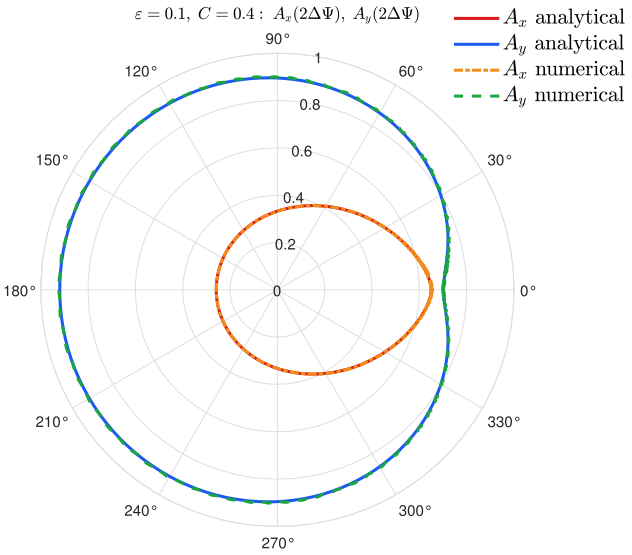

Fig. 11 Comparison of the analytical vs. numerical solution in polar coordinates for $X_0 = 0.65$, $U_0 = 0$, $Y_0 = 0.70$, and $V_0 = 0$

A_0^2. Therefore, for a given Δ_Ψ, either 0 or 2 positive real solutions for A_y in Eq. (46) exist.

Remark 6 Not for all values of Δ_Ψ is A_y real. The existence condition of real A_y for all Δ_Ψ follows from the non-negativeness of the inner square root and is given by

$$2C \leq \frac{3}{2} + \frac{8\Phi_0}{A_0^4}. \tag{49}$$

Graphical examples are given in Figs. 10-11 for the two different cases. In Fig. 10, the phase difference Δ_Ψ is limited to an interval within $[0, 2\pi)$, outside of which no real A_y exists. Here, the two modes A_x and A_y are identical, although shifted in time. The situation is different in Fig. 11, where, despite energy exchange, one of the amplitudes remains always smaller than the other, yielding an asymmetrical scenario. For validation, the numerical solutions of Eqs. (18)-(19) are also converted to amplitude and phase shift coordinates, showing a good agreement with the explicit analytical results.

3.2 Level-crossing event

For a level-crossing event, one of the amplitudes, A_x or A_y, must reach the critical distance, $d_{\mathrm{cr}} = 1$. In the limiting case, the trajectory of the particle, and thus $A_x(\Delta_\Psi)$ or $A_y(\Delta_\Psi)$, is tangential to the line $A_x = 1$ or $A_y = 1$, respectively, i.e., the derivative vanishes.

$$\frac{\mathrm{d}A_y}{\mathrm{d}\Delta_\Psi} = 0 \quad \Rightarrow \quad A_y(A_0^2 - A_y^2)\sin(2\Delta_\Psi) = 0. \tag{50}$$

Since we are interested only in the nondegenerate solutions, where $A_x A_y \neq 0$, Eq. (50) is fulfilled if $2\Delta_\Psi = k\pi$ with $k = \{0, 1\}$. Tangency to $A_x = 1$, i.e. $\frac{\mathrm{d}A_x}{\mathrm{d}\Delta_\Psi} = 0$ yields the same condition.

Regarding level crossing, the larger amplitude, $A_{y,1} = A_{x,2}$ matters. If condition (49) holds, we can easily convince ourselves that $A_{y,1} = A_{x,2}$ takes its maximum at $2\Delta_\Psi = \pi$ and its minimum at 0, respectively (cf. Fig. 11). If condition (49) does not hold, at zero, no real amplitude exists. The maximum, however, is still taken at $2\Delta_\Psi = \pi$ (cf. Fig. 10).

3.3 Insertion of the ICs

It remains to convert ICs X_0, Y_0, U_0, V_0 to ICs in $A_{y,0}$ and $\Delta_{\Psi,0}$ to determine the value of Φ_0. Considering general ICs, i.e.,

$$A_{x,0} = \sqrt{X_0^2 + U_0^2}, \quad \Psi_{x,0} = \mathrm{atan2}(X_0, U_0), \tag{51}$$

$$A_{y,0} = \sqrt{Y_0^2 + V_0^2}, \quad \Psi_{y,0} = \mathrm{atan2}(Y_0, V_0). \tag{52}$$

We can write the constants as

$$\begin{aligned}\Delta_{\Psi,0} = \Psi_{1,0} - \Psi_{2,0} &= \arctan\frac{X_0}{U_0} - \arctan\frac{Y_0}{V_0} \\ &= \arctan\frac{X_0V_0 - Y_0U_0}{X_0Y_0 + U_0V_0}.\end{aligned} \tag{53}$$

Then, using the identities

$$\cos(2x) = 2\cos^2 x - 1 \quad \text{and} \quad \cos^2\arctan(x) = \frac{1}{1+x^2}, \tag{54}$$

we have

$$\cos(2\Delta_{\Psi,0}) = \frac{(X_0Y_0 + U_0V_0)^2 - (X_0V_0 - U_0Y_0)^2}{(X_0^2 + U_0^2)(Y_0^2 + V_0^2)}. \quad (55)$$

and

$$A_{y,0}^2\left(A_0^2 - A_{y,0}^2\right) = A_{x,0}^2 A_{y,0}^2 = (X_0^2 + U_0^2)(Y_0^2 + V_0^2) \quad (56)$$

which yields

$$\Phi_0 = \left(C - \frac{3}{4}\right)(X_0^2 + U_0^2)(Y_0^2 + V_0^2) + \frac{C}{2}\left((X_0Y_0 + U_0V_0)^2 - (X_0V_0 - U_0Y_0)^2\right). \quad (57)$$

The extremum of Eq. (46), $\tilde{A}_y$ (or equivalently $\tilde{A}_x$) is given at $2\Delta_\Psi = \pi$ by

$$\Phi_0(\tilde{A}_y, \Delta_\Psi = \pi/2) = \left(C - \frac{3}{4} - \frac{C}{2}\right)\tilde{A}_y^2\left(A_0^2 - \tilde{A}_y^2\right) = \frac{1}{4}(2C - 3)\,\tilde{A}_y^2\left(A_0^2 - \tilde{A}_y^2\right). \quad (58)$$

At this point, the largest ℓ^∞ distance of the particle from the origin during its trajectory is reached. In the case of a level crossing $\tilde{A}_y = 1$, thus, after insertion of the ICs from Eq. (57) in Eq. (58), we get the formula for the boundary of the safe basin

$$X_0^2 + Y_0^2 + U_0^2 + V_0^2 - \frac{3 - 6C}{3 - 2C}\left(X_0^2Y_0^2 + U_0^2V_0^2\right) - X_0^2V_0^2 - Y_0^2U_0^2 + \frac{8C}{3 - 2C}X_0Y_0U_0V_0 = 1 \quad (59)$$

With zero-velocity ICs, the boundary becomes

$$X_0^2 + Y_0^2 - \frac{3 - 6C}{3 - 2C}X_0^2Y_0^2 = 1. \quad (60)$$

Fig. (7b) shows an example of the analytically obtained boundary for fixed $U_0 = V_0 = 0$ with $C = 0.2$ for the level-crossing problem with $SF = 1.25$ ($\varepsilon = 0.64$). Figures 12–13 show sections of the SBOLC in 3D space for some values of V_0 and C.

4 The volume of the SBOLC

We aim to compute the volume of the bounded domain in four-dimensional space defined implicitly by Eq. (59). To facilitate the computation of the volume, we transform the

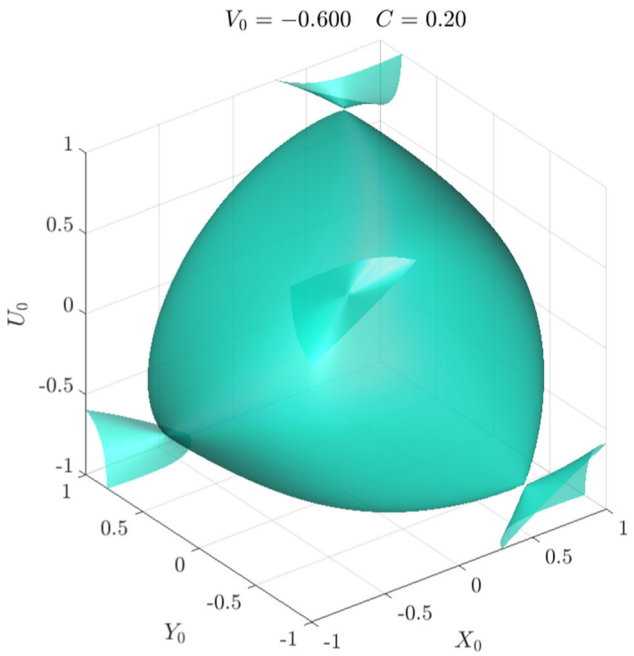

Fig. 12 SBOLC for $C = 0.2$ and $V_0 = -0.6$. An animated version of this figure is available in the Electronic Supplementary Material (`basin_sections.mp4`)

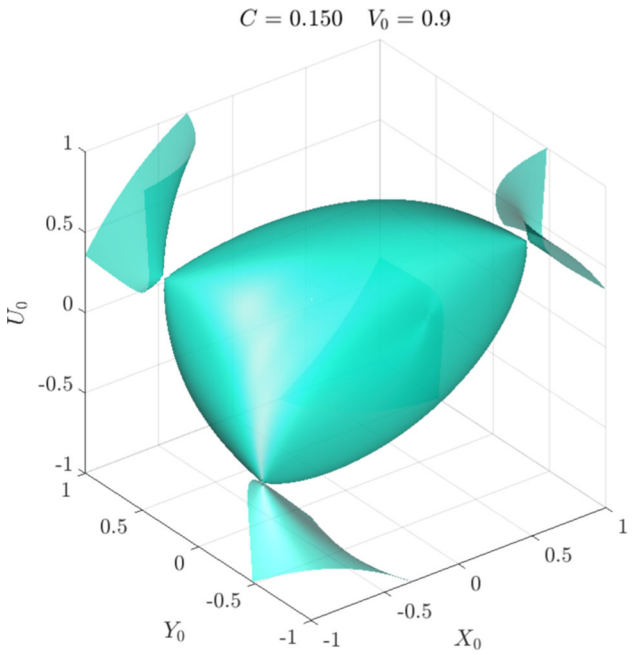

Fig. 13 SBOLC for $C = 0.15$ and $V_0 = 0.9$. An animated version of this figure is available in the Electronic Supplementary Material (`basin_vs_C.mp4`)

Cartesian coordinates (X_0, Y_0, U_0, V_0) into 4D hyperspherical coordinates $(r, \theta_1, \theta_2, \theta_3)$:

$$X_0 = r\sin\theta_1\sin\theta_2\sin\theta_3, \quad (61)$$
$$Y_0 = r\sin\theta_1\sin\theta_2\cos\theta_3, \quad (62)$$
$$U_0 = r\sin\theta_1\cos\theta_2, \quad (63)$$

$$V_0 = r\cos\theta_1, \tag{64}$$

with the ranges:

$$r \geq 0, \quad \theta_1 \in [0, \pi], \quad \theta_2 \in [0, \pi], \quad \theta_3 \in [0, 2\pi].$$

The volume element in 4D hyperspherical coordinates is given by:

$$\mathrm{d}V = r^3 \sin^2\theta_1 \sin\theta_2 \mathrm{d}r\mathrm{d}\theta_1\mathrm{d}\theta_2\mathrm{d}\theta_3. \tag{65}$$

Substituting the transformations from Eqs. (61)-(64) into the implicit Eq. (59), we simplify the expression step by step. First, note that:

$$X_0^2 + Y_0^2 + U_0^2 + V_0^2 = r^2. \tag{66}$$

We then compute the terms involving products of variables:

$$X_0^2 Y_0^2 = r^4 \sin^4\theta_1 \sin^4\theta_2 \sin^2\theta_3 \cos^2\theta_3, \tag{67}$$
$$U_0^2 V_0^2 = r^4 \sin^2\theta_1 \cos^2\theta_1 \cos^2\theta_2, \tag{68}$$
$$X_0^2 V_0^2 = r^4 \sin^2\theta_1 \cos^2\theta_1 \sin^2\theta_2 \sin^2\theta_3, \tag{69}$$
$$U_0^2 Y_0^2 = r^4 \sin^4\theta_1 \sin^2\theta_2 \cos^2\theta_2 \cos^2\theta_3, \tag{70}$$
$$X_0 Y_0 U_0 V_0 = r^4 \sin^3\theta_1 \cos\theta_1 \sin^2\theta_2 \cos\theta_2 \sin\theta_3 \cos\theta_3. \tag{71}$$

For brevity, define the following functions:

$$A'(\theta_1, \theta_2, \theta_3) = \sin^4\theta_1 \sin^4\theta_2 \sin^2\theta_3 \cos^2\theta_3 + \sin^2\theta_1 \cos^2\theta_1 \cos^2\theta_2, \tag{72}$$
$$B'(\theta_1, \theta_2, \theta_3) = \sin^2\theta_1 \cos^2\theta_1 \sin^2\theta_2 \sin^2\theta_3 + \sin^4\theta_1 \sin^2\theta_2 \cos^2\theta_2 \cos^2\theta_3, \tag{73}$$
$$D'(\theta_1, \theta_2, \theta_3) = \sin^3\theta_1 \cos\theta_1 \sin^2\theta_2 \cos\theta_2 \sin\theta_3 \cos\theta_3. \tag{74}$$

Then, define:

$$F(\theta_1, \theta_2, \theta_3) = \frac{3 - 6C}{3 - 2C} A' + B' - \frac{8C}{3 - 2C} D'. \tag{75}$$

Substituting back into Eq. (59), we have:

$$F(\theta_1, \theta_2, \theta_3) r^4 - r^2 + 1 = 0. \tag{76}$$

Let $s = r^2$, the equation becomes a quadratic in s:

$$Fs^2 - s + 1 = 0. \tag{77}$$

In the selected parameter range of C, both solutions of Eq. (77) are real and positive. Thus, we consider only the smaller one, which describes the safe basin boundary

$$s = \frac{1 - \sqrt{1 - 4F}}{2F}. \tag{78}$$

Thus,

$$r_{\max} = \sqrt{s}. \tag{79}$$

The volume V of the shape is given by

$$V = \frac{1}{4} \int_0^{\pi} \int_0^{\pi} \int_0^{2\pi} r_{\max}^4(\theta_1, \theta_2, \theta_3) \sin^2\theta_1 \sin\theta_2 \, \mathrm{d}\theta_1 \, \mathrm{d}\theta_2 \, \mathrm{d}\theta_3. \tag{80}$$

Recall that $s = r_{\max}^2$ is the smaller root of the quadratic equation

$$Fs^2 - s + 1 = 0, \tag{81}$$

which gives

$$s = r_{\max}^2(\theta_1, \theta_2, \theta_3) = \frac{1 - \sqrt{1 - 4F(\theta_1, \theta_2, \theta_3)}}{2F(\theta_1, \theta_2, \theta_3)}. \tag{82}$$

For $|F| < 1/4$ this expression admits the convergent power series

$$r_{\max}^2 = \sum_{n=0}^{\infty} C_n F^n, \tag{83}$$

where C_n are the Catalan numbers

$$C_n = \frac{1}{n+1}\binom{2n}{n}, \qquad n = 0, 1, 2, \ldots \tag{84}$$

and $F = F(\theta_1, \theta_2, \theta_3)$ is given in Eq. (75). Squaring this series yields

$$r_{\max}^4 = \left(r_{\max}^2\right)^2 = \left(\sum_{n=0}^{\infty} C_n F^n\right)^2 = \sum_{k=0}^{\infty} \left(\sum_{n=0}^{k} C_n C_{k-n}\right) F^k. \tag{85}$$

Using the classical convolution identity for Catalan numbers [49],

$$\sum_{n=0}^{k} C_n C_{k-n} = C_{k+1}, \tag{86}$$

we obtain the compact representation

$$r_{\max}^4 = \sum_{k=0}^{\infty} C_{k+1} F^k. \tag{87}$$

Inserting this into Eq. (80) gives

$$V = \frac{1}{4}\sum_{k=0}^{\infty} C_{k+1} \int_0^{\pi}\int_0^{\pi}\int_0^{2\pi} F(\theta_1,\theta_2,\theta_3)^k \sin^2\theta_1 \sin\theta_2 \,\mathrm{d}\theta_1 \,\mathrm{d}\theta_2 \,\mathrm{d}\theta_3. \tag{88}$$

Each coefficient in the series (88) is an angular moment of F^k on the four-dimensional unit sphere and can, in principle, be reduced to a finite combination of beta function integrals. However, the resulting expressions become rapidly unwieldy and no simple closed form for $V(C)$ appears to be available.

In practice we therefore evaluate $V(C)$ numerically. On the one hand we compute the integral (80) directly by Gauss–Legendre quadrature in the angular variables. On the other hand we use the series representation (88) truncated at a finite order $k_{\max}$. The two approaches agree to numerical accuracy for moderate $k_{\max}$, which confirms the consistency of the derivation (see Fig. 14).

For zero velocity ICs, the area of the safe basin in the parameter region $C = [0, 0.5]$ can be calculated in an exact form by expressing $Y_0(X_0)$ and using the four-fold mirror symmetry.

$$\begin{aligned}\mathrm{Area}(SBOLC) &= 4\int_0^1 \sqrt{\frac{1-x^2}{1-\frac{3-6C}{3-2C}x^2}}\,\mathrm{d}x \\ &= \sqrt{\frac{3-2C}{3-6C}}\,E\left(\sqrt{\frac{3-6C}{3-2C}}, \sqrt{\frac{3-2C}{3-6C}}\right).\end{aligned} \tag{89}$$

4.1 Analytic lower bound on the 4D SBOE

In this section, we give a simple analytic lower estimate on the volume of the SBOE, considering the simple fact that escape is only possible if the particle's total initial energy reaches the energy of the saddles, located at $(\pm 1, 0)$ and $(0, \pm 1)$. The potential energy at these points is $1/4$. The safe basin is thus given by the inequality:

$$V(\mathbf{x_0}) + T(\mathbf{x_0}) \le \frac{1}{4}, \tag{90}$$

$$\frac{x_0^2}{2} + \frac{y_0^2}{2} - \frac{x_0^4}{4} - \frac{y_0^4}{4} - Cx_0^2y_0^2 + \frac{u_0^2}{2} + \frac{v_0^2}{2} \le \frac{1}{4}. \tag{91}$$

The hypervolume can be calculated by a four-dimensional integral. We note that

$$\frac{u_0^2}{2} + \frac{v_0^2}{2} \le \underbrace{\frac{1}{4} - \frac{x_0^2}{2} - \frac{y_0^2}{2} + \frac{x_0^4}{4} + \frac{y_0^4}{4} + Cx_0^2y_0^2}_{=:F(x_0,y_0;C)} \tag{92}$$

is a disk with radius $\sqrt{2F(x_0, y_0; C)}$ for fixed values x and y, thus has an area of

$$A(x_0, y_0; C) = 2\pi F(x_0, y_0; C). \tag{93}$$

The lower estimate of the safe basin's area can thus be given by

$$V_L = \iint_D A(x_0, y_0; C)\mathrm{d}x\mathrm{d}y = 2\pi \iint_D F(x_0, y_0; C)\mathrm{d}x\mathrm{d}y, \tag{94}$$

where D is given by

$$D := \left\{(x, y) \in \mathbb{R}^2 \,\middle|\, V(x, y) < \frac{1}{4}\right\}. \tag{95}$$

For easier handling, we switch to polar coordinates.

$$x = r\cos\varphi, \qquad y = r\sin\varphi, \tag{96}$$

with

- $x^2 + y^2 = r^2$,
- $x^4 + y^4 = r^4(\cos^4\varphi + \sin^4\varphi) = r^4\left(1 - \frac{\sin^2 2\varphi}{2}\right)$,
- $x^2y^2 = r^4\cos^2\varphi\sin^2\varphi = \frac{r^4}{4}\sin^2 2\varphi$.

We rewrite $F(x_0, y_0)$ as follows.

$$\begin{aligned}F(r,\varphi) &= \frac{1}{4} - \frac{r^2}{2} + \frac{r^4}{4}\left(1 - \frac{\sin^2 2\varphi}{2}\right) + C\frac{r^4}{4}\sin^2 2\varphi \\ &= \left(\frac{1}{4} - \frac{r^2}{2} + \frac{r^4}{4}\right) - \frac{r^4}{8}\underbrace{(1-2C)}_{=:k}\sin^2 2\varphi\end{aligned}$$

The boundary of D is defined by

$$F(R(\varphi), \varphi) = 0, \tag{97}$$

$$\left(2 - k\sin^2 2\varphi\right)R^4(\varphi) - 4R^2(\varphi) + 2 = 0, \tag{98}$$

yielding the solutions

$$\begin{aligned}R_{1,2}^2(\varphi) &= \frac{4 \pm \sqrt{16 - 8(2 - k\sin^2 2\varphi)}}{2(2 - k\sin^2 2\varphi)} \\ &= \frac{2 - \sqrt{2k}|\sin 2\varphi|}{2 - k\sin^2 2\varphi},\end{aligned} \tag{99}$$

where we chose the solution with the minus sign, as this expression corresponds to the inner equipotential level set.

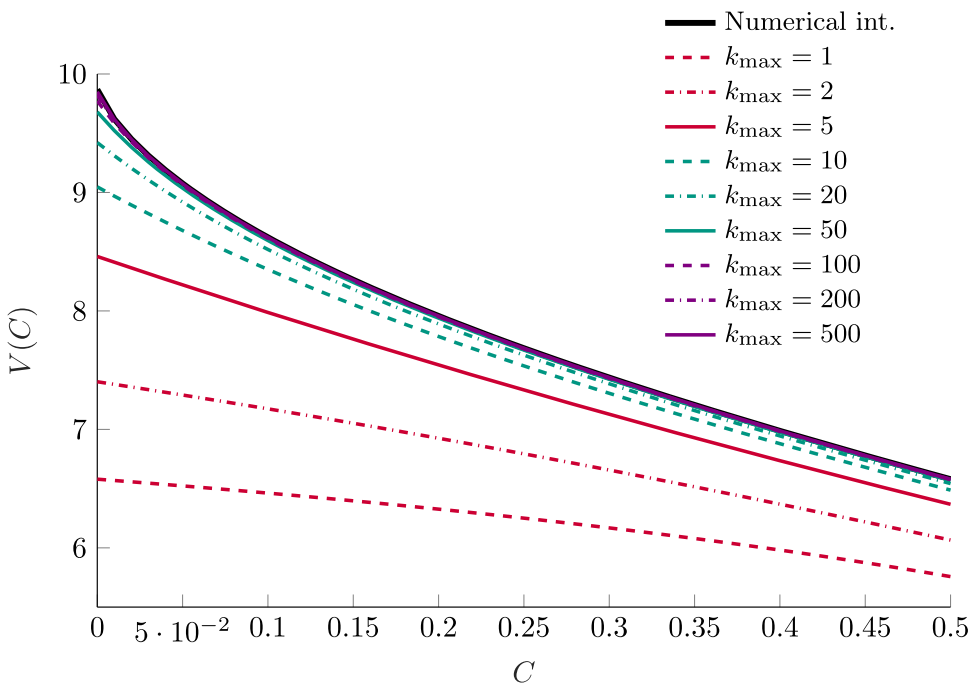

Fig. 14 Convergence of the Catalan numbers-based series solution to the direct numerical quadrature of Eq. (80)

Thus, Eq. (94) can be rewritten in polar coordinates as follows.

$$V_L = 2\pi \int_0^{2\pi} \int_0^{R(\varphi)} F(r, \varphi; C) r \mathrm{d}r \mathrm{d}\varphi, \tag{100}$$

$$= 2\pi \int_0^{2\pi} \int_0^{R(\varphi)} \left(\frac{1}{4} - \frac{r^2}{2} + \frac{r^4}{4} - \frac{r^4}{8} k \sin^2 2\varphi \right) r \mathrm{d}r \mathrm{d}\varphi \tag{101}$$

$$= 2\pi \int_0^{2\pi} \frac{R^2(\varphi)}{8} - \frac{R^4(\varphi)}{8} + \frac{R^6(\varphi)}{24} - k \sin^2 2\varphi \frac{R^6(\varphi)}{48} \mathrm{d}\varphi \tag{102}$$

$$= 2\pi \int_0^{\pi/4} R^2(\varphi) - R^4(\varphi) + \frac{R^6(\varphi)}{3} - k \sin^2 2\varphi \frac{R^6(\varphi)}{6} \mathrm{d}\varphi, \tag{103}$$

where in the last line, we used the eight-fold symmetry of the boundary.

Omitting the details of the integration, the formula representing the lower estimate on the hypervolume of the safe basin is given by

$$V_L(k) = \sqrt{2}\pi \frac{\sqrt{(2-k)k} + (1-k) \arccos(k-1)}{3(2-k)^{3/2}}. \tag{104}$$

Alternatively, in terms of C, the hypervolume is given by

$$V_L(C) = \sqrt{2}\pi \frac{\sqrt{1-4C^2} + 2C \arccos(-2C)}{3(1+2C)^{3/2}}. \tag{105}$$

See Fig. 17a for a graphical representation. Note that this estimate is very conservative, as it is based on limited information about the system's dynamics. Unlike Eq. (80), Eq. (105) does not consider the mechanisms of energy exchange between the modes at all.

4.2 Analytic lower bound for the 2D safe-basin area

The calculation of the area enclosed by the inner equipotential curve $V(x_0, y_0) = 1/4$ is analogous to the derivation carried out in the previous subsection for the four–dimensional lower estimate. Switching to polar coordinates and selecting the inner root of the corresponding quadratic equation again yields a radius function $r = R(\varphi)$, describing the closed component surrounding the origin. Repeating the same steps as before, but now integrating only over the (x_0, y_0)–plane, leads after simplification to the final expression

$$A_L(C) = \frac{\sqrt{2}}{\sqrt{1+2C}} \arccos(-2C), \qquad 0 \le C \le \frac{1}{2}, \tag{106}$$

providing the lower bound on the area of the two-dimensional safe basin at the potential level $V = 1/4$. For a graphical representation, see Fig. 17b .

5 Numerical validation with Monte Carlo simulation

For validation of the analytical calculations, the safe basin volume within the initial-condition hypercube $H_d = [-1, 1]^d$

was estimated by Monte Carlo sampling combined with percentile bootstrap for each value of C. In the zero-velocity case, $(U_0, V_0) = (0, 0)$ and therefore $d = 2$ with $|H_2| = 4$. For the full four-dimensional case $d = 4$ and $|H_4| = 16$.

The sampling was performed in N_b independent batches, each containing n initial conditions. Within each batch, the initial conditions were drawn uniformly from H_d, and the system (18)–(19) was integrated with an event that stopped the solver when $\max\{|X(t)|, |Y(t)|\} = 1$ or when $t = T_{\max}$. For each trajectory, an indicator I_i was recorded, equal to 1 if the trajectory did not reach the boundary and 0 otherwise. The hypervolume estimate for one batch was computed as

$$\widehat{V}_b = |H_d| \cdot \frac{1}{n} \sum_{i=1}^{n} I_i,$$

and the overall Monte Carlo estimate was taken as the mean of the batch results,

$$\widehat{V} = \frac{1}{N_b} \sum_{b=1}^{N_b} \widehat{V}_b.$$

To quantify the statistical uncertainty, a bootstrap resampling was applied over the batch estimates [50]. From the set of $\{\widehat{V}_b\}_{b=1}^{N_b}$, B bootstrap samples were generated by resampling with replacement. For each resample the average $\widehat{V}^{*(k)}$ was computed, and the 2.5th and 97.5th percentiles of $\{\widehat{V}^{*(k)}\}_{k=1}^{B}$ were used to form the 95% confidence interval.

All integrations were carried out using `ode45` with event detection at $\max\{|X|, |Y|\} - 1 = 0$, absolute and relative tolerances of 10^{-8}, final time $T_{\max}$, and a fixed random seed for reproducibility. In each case, $T_{\max}$ was chosen large enough (100, 500, or 2000) to have no influence on the simulation results. This was achieved by checking manually that the half-time period of beating (see Figs. 8 and 9) is shorter than $T_{\max}$.

5.1 Accuracy of the analytical SBOLC for finite ε

The analytical construction of the SBOLC relies on the small parameter $\varepsilon = 1/SF^2$. To evaluate its practical validity, we compared the analytical safe basin with Monte Carlo simulations of the full system in three representative regimes; the results are shown in Figs. 15,16, and 17.

For $\varepsilon = 0.05$ ($SF \approx 4.47$) (weakly nonlinear level crossing), the agreement is excellent, both for the four–dimensional basin volume and for the two-dimensional displacement plane $(U_0, V_0) = (0, 0)$ (cf. Figs. 15a and 16a).

For $\varepsilon = 0.2$ ($SF \approx 2.23$) (moderately nonlinear), the analytical method starts to *overestimate* the size of the safe basin. This effect is apparent in four dimensions, whereas in the two-dimensional displacement plane the discrepancy remains small cf. Figs. 15b and 16b.

For $\varepsilon = 1$ ($SF = 1$) (strongly nonlinear escape), the analytical prediction substantially overestimates the safe basin in both 4D and 2D. In this regime, the small–parameter assumption is no longer valid (cf. Fig. 17).

Thus, the method is quantitatively accurate only for sufficiently small ε. As ε increases, nonlinear effects reduce the validity of the averaging and lead to an overestimation of the safe basin.

5.2 Practical choice of the *SF*

The averaging method is justified for small nonlinearities. With its use, we can describe the evolution of the system when both modes have approximately the same frequency. Numerical simulations show that as we approach the boundary of the potential well, other types of trajectories appear, including stable periodic orbits with an $n : m$ frequency ratio, surrounded by their safe basins (cf. Fig. 5). Moving even closer, the dynamics become increasingly chaotic, and analytical treatment becomes impractical. Therefore, identifying an adequate safety factor, such that the corresponding SBOLC includes a large portion of the SBOE without containing any escaping initial conditions, is crucial. As shown in Figs. 15-17, the analytically determined SBOLC overestimates the actual size of the safe basin. Consequently, for small SF values (large ε), many ICs will escape in reality, even though they are within the analytical SBOLC. Fig. 18 presents a numerical study where, for different SF values, randomly generated initial conditions from the corresponding SBOLC were used in simulations. The fraction of escaping initial conditions and the total number of initial conditions are shown for different values of C and SF. It transpires that an SF of 1.5 provides complete safety against escape.

6 Conclusions and scope for future research

The dynamics of particles in a bi-quartic potential well were investigated, focusing on the safe basins of escape and level crossing. Energy exchange between modes is facilitated by a coupling term, leading to a complex dependence of escape on initial conditions. An analytical approach based on averaging and slow manifold transformations was employed to reduce the fourth-order system to a first-order one. This reduction enabled us to derive an additional conservation law in the averaged system, helping to determine the safe basin boundary and its volume. The analytical estimates provide direct information on the effects of initial conditions on escape and level crossing, enabling a more straightforward design of robust engineering applications. This study also advances the results of *Engel et al.* [41]. Their investigation

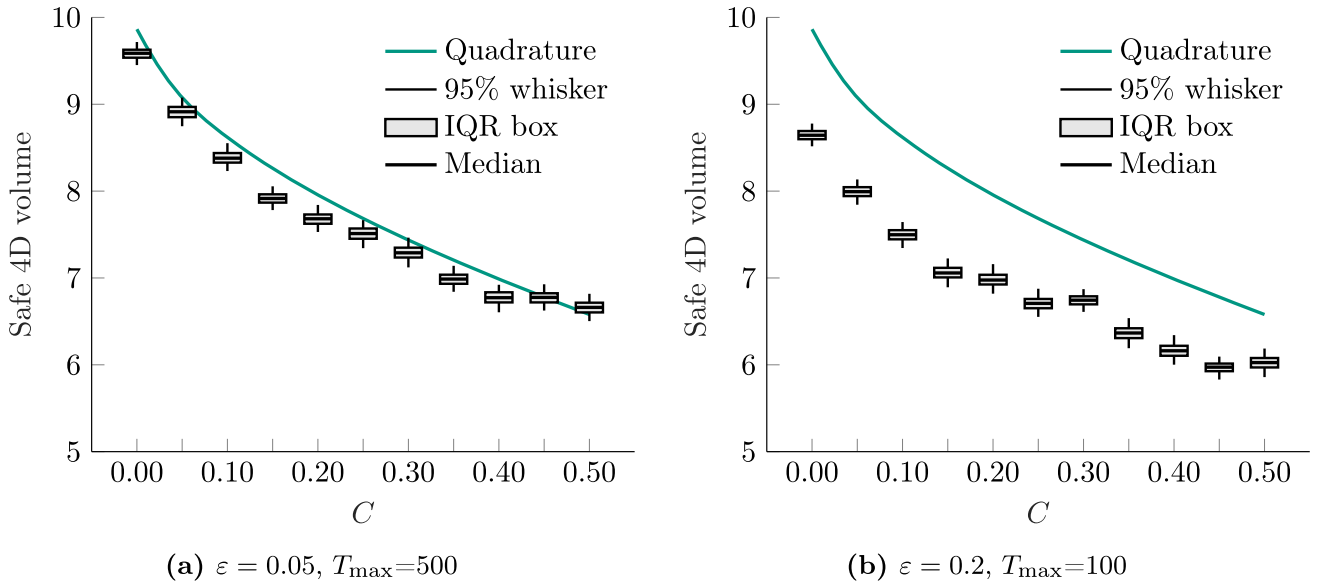

(a) $\varepsilon = 0.05$, $T_{\max}$=500 **(b)** $\varepsilon = 0.2$, $T_{\max}$=100

Fig. 15 Comparison of the four-dimensional hypervolume of the safe basin given by Eq. (80) and the result of numerical Monte Carlo simulations with batch size $N_b = 100$ and sample size $n = 100$ depicted against the detuning parameter C for different values of ε

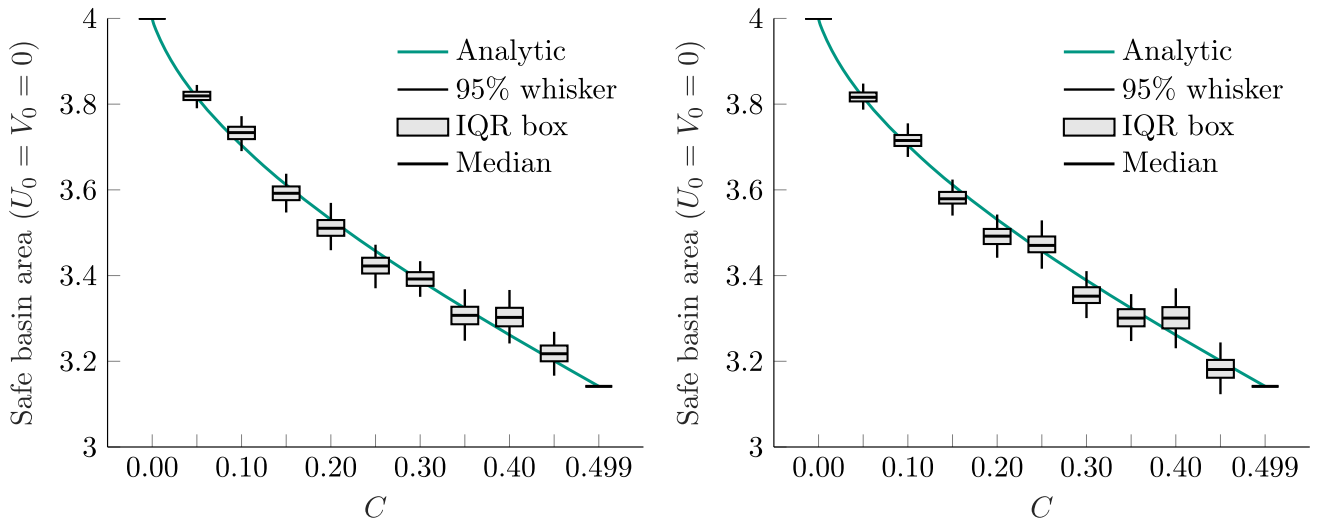

(a) $\varepsilon = 0.05$, $T_{\max}$=2000 **(b)** $\varepsilon = 0.2$, $T_{\max}$=500

Fig. 16 Comparison of the two-dimensional area of the safe basin given by Eq. (89) and the result of numerical Monte Carlo simulations with batch size $N_b = 50$ and sample size $n = 50$ depicted against the detuning parameter C for different values of ε

was extended by considering non-zero initial velocity conditions; thus, this study provides a more precise approximation of the safe basin.

The analytical expression derived for the safe basin boundary offers a novel insight into escape dynamics in a four-dimensional phase space and provides an alternative to purely numerical methods. The findings have the potential to be extended to broader applications, including celestial mechanics, ship dynamics, and MEMS stability, where similar escape and level-crossing phenomena occur. Future explorations should include systems with external forcing, in which case the total energy is not conserved, potentially preventing an exact analytical solution for the slow system. In the case of damped systems, even the additional first integral of the slow system might not exist; thus, alternative analytical techniques must be used. However, as damping increases, the initial conditions become less important as transients decay faster. Therefore, a search for safe basins is less justified. Although some form of damping is almost always present in technically relevant cases, conservative models tend to provide worst-case scenarios for safe basins, underscoring the importance of this current investigation.

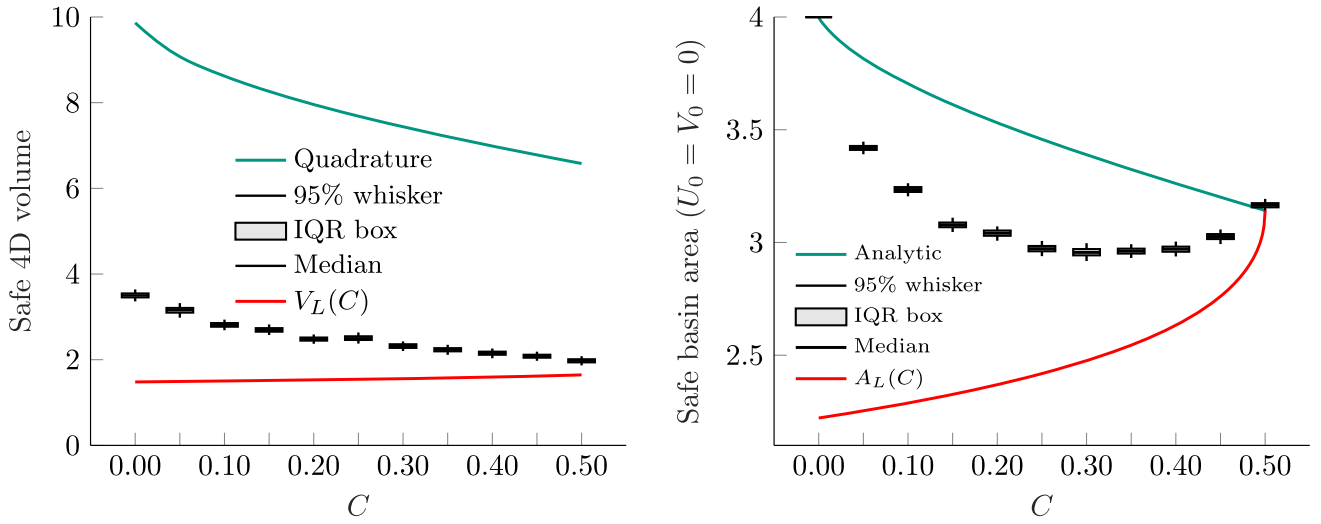

(a) 4D volume with general IC, $T_{\max}$=100 **(b)** 2D volume with zero-velocity IC, $T_{\max}$=100

Fig. 17 Comparison of the two- and four-dimensional size of the safe basins to the result of numerical Monte Carlo simulations with batch size $N_b = 100$ and sample size $n = 100$ depicted against the detuning parameter C for the original escape problem with large non-linearity, $\varepsilon = 1$

Fig. 18 Fraction of escaping ICs when chosen from the four-dimensional SBOLC at a given SF value. $T_{\max} = 200$. Sample size $N = 3000$

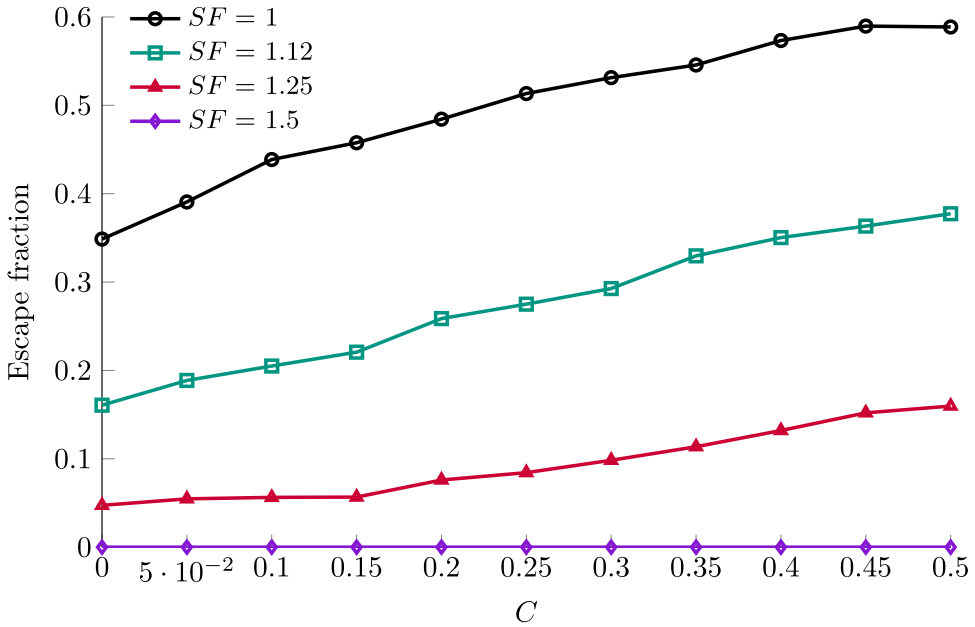

Appendix A Stability of fix points and periodic orbits

We investigate the stability of the steady-state and partially steady-state solutions of Eqs. (34)–(41), i.e., the periodic solutions of Eqs. (22)–(23).

$$f_1(A_x, A_y, \Delta_\Psi) = -\frac{CA_xA_y^2}{4}\sin\big(2\Delta_\Psi\big), \tag{A1}$$

$$f_2(A_x, A_y, \Delta_\Psi) = \frac{CA_x^2A_y}{4}\sin\big(2(\Delta_\Psi)\big), \tag{A2}$$

$$f_3(A_x, A_y, \Delta_\Psi) = \frac{A_x^2-A_y^2}{2}\Big(-\frac{3}{4}+C\big(1+\frac{1}{2}\cos(2\Delta_\Psi)\big)\Big). \tag{A3}$$

The Jacobian is given by

$$J = \begin{pmatrix} \frac{\partial f_1}{\partial A_x} & \frac{\partial f_1}{\partial A_y} & \frac{\partial f_1}{\partial \Delta_\Psi} \\ \frac{\partial f_2}{\partial A_x} & \frac{\partial f_2}{\partial A_y} & \frac{\partial f_2}{\partial \Delta_\Psi} \\ \frac{\partial f_3}{\partial A_x} & \frac{\partial f_3}{\partial A_y} & \frac{\partial f_3}{\partial \Delta_\Psi} \end{pmatrix} \tag{A4}$$

$$J = \begin{pmatrix} -\frac{CA_y^2}{4}\sin\big(2\Delta_\Psi\big) & -\frac{CA_xA_y}{2}\sin\big(2\Delta_\Psi\big) & -\frac{CA_xA_y^2}{2}\cos\big(2\Delta_\Psi\big) \\ \frac{CA_xA_y}{2}\sin\big(2\Delta_\Psi\big) & \frac{CA_x^2}{4}\sin\big(2\Delta_\Psi\big) & \frac{CA_x^2A_y}{2}\cos\big(2\Delta_\Psi\big) \\ A_x\Big(-\frac{3}{4}+C\big(1+\frac{1}{2}\cos(2\Delta_\Psi)\big)\Big) & -A_y\Big(-\frac{3}{4}+C\big(1+\frac{1}{2}\cos(2\Delta_\Psi)\big)\Big) & -\frac{C(A_x^2-A_y^2)}{2}\sin\big(2\Delta_\Psi\big) \end{pmatrix}. \tag{A5}$$

Appendix A.1 Diagonal oscillations

We evaluate the Jacobian at $A_x = A_y = A_0$ and $\Delta_\Psi = 0$

$$J\big(A_0, A_0, 0\big) = \begin{pmatrix} 0 & 0 & -\frac{CA_0^3}{2} \\ 0 & 0 & \frac{CA_0^3}{2} \\ -A_0M & A_0M & 0 \end{pmatrix}, \tag{A6}$$

with

$$M = \frac{3}{4}\big(1-2C\big). \tag{A7}$$

For convenience, we set

$$\alpha = \frac{CA_0^3}{2}, \quad \text{and} \quad \beta = A_0M = A_0\frac{3}{4}\big(1-2C\big). \tag{A8}$$

Then,

$$|J\big(A_0, A_0, 0\big)| = \det\begin{vmatrix} 0 & 0 & -\alpha \\ 0 & 0 & \alpha \\ -\beta & \beta & 0 \end{vmatrix} = 0. \tag{A9}$$

We seek eigenvalues λ by solving $\det\big(J-\lambda I\big) = 0$. Thus

$$J - \lambda I = \begin{pmatrix} -\lambda & 0 & -\alpha \\ 0 & -\lambda & \alpha \\ -\beta & \beta & -\lambda \end{pmatrix}. \tag{A10}$$

A direct expansion gives the characteristic polynomial

$$\chi(\lambda) = -\lambda\big(\lambda^2 - 2\alpha\beta\big), \tag{A11}$$

with the eigenvalues:

$$\lambda_1 = 0, \qquad \lambda_{2,3} = \pm\sqrt{2\alpha\beta}. \tag{A12}$$

Since

$$\alpha = \frac{CA_0^3}{2} > 0, \quad \text{and} \quad \beta = A_0\frac{3}{4}\big(1-2C\big) > 0, \tag{A13}$$

there exists a positive root, leading to an unstable solution.

Appendix A.2 Circular orbit

We evaluate the Jacobian at $A_x = A_y = A_0$ and $\Delta_\Psi = \frac{\pi}{2}$:

$$J\left(A_0, A_0, \frac{\pi}{2}\right) = \begin{pmatrix} 0 & 0 & \frac{CA_0^3}{2} \\ 0 & 0 & -\frac{CA_0^3}{2} \\ -A_0M & A_0M & 0 \end{pmatrix}, \tag{A14}$$

with

$$M = \frac{3}{4} - \frac{C}{2}. \tag{A15}$$

Defining

$$\alpha = \frac{C A_0^3}{2} \quad \text{and} \quad \beta = A_0 M = A_0\Big(\frac{3}{4} - \frac{C}{2}\Big), \tag{A16}$$

the Jacobian becomes:

$$J\Big(A_0, A_0, \frac{\pi}{2}\Big) = \begin{pmatrix} 0 & 0 & +\alpha \\ 0 & 0 & -\alpha \\ -\beta & +\beta & 0 \end{pmatrix}. \tag{A17}$$

Thus, the characteristic polynomial is

$$\chi(\lambda) = -\lambda\Big(\lambda^2 + 2\alpha\beta\Big), \tag{A18}$$

whose roots are

$$\lambda_1 = 0, \quad \lambda_{2,3} = \pm i\sqrt{2\alpha\beta}. \tag{A19}$$

Since $\alpha > 0$ and $\beta > 0$, the system does not have any roots with positive real parts, which would otherwise indicate instability. However, marginal stability cannot be determined because the analysis was conducted on a linearized system with eigenvalues of zero real part. Therefore, according to Hartmann-Grobman's theorem, the linear stability analysis does not provide a definitive conclusion on stability. However, numerical simulations show that perturbations of the near-circular orbit remain bounded for $L \in \mathcal{O}(\sqrt{\varepsilon})$ (cf. Sect. 2) and only become unstable for $L \in \mathcal{O}(1)$.

$$A_x^*(\tau) = A_0 \tag{A20}$$

$$A_y^*(\tau) = 0 \tag{A21}$$

$$\Delta_\Psi^*(\tau) = -\arctan\left[\sqrt{\frac{6C-3}{2C-3}}\,\tan\left(\sqrt{\Big(C-\frac{3}{4}\Big)^2 - \Big(\frac{C}{2}\Big)^2}\left(\frac{A_0^2}{2}\tau - K_0\right)\right)\right], \tag{A22}$$

with

$$K_0 = \frac{\tan^{-1}\left[\sqrt{\frac{2C-3}{6C-3}}\,\tan\left(\Delta_{\Psi,0}\right)\right]}{\sqrt{\Big(C-\frac{3}{4}\Big)^2 - \Big(\frac{C}{2}\Big)^2}} \tag{A23}$$

Since $A_y = 0$, it is irrelevant what Ψ_y is, thus, we can assume an arbitrary $\Psi_{y,0}$ including $\Psi_{y,0} = \Psi_{x,0}$. In which case $K_0 = 0$. This solution is periodic, and its stability analysis requires determining the Floquet multipliers. To analyze the stability of the above solution, we introduce small perturbations:

$$A_x(\tau) = A_0 + \delta A_x(\tau), \tag{A24}$$

$$A_y(\tau) = 0 + \delta A_y(\tau), \tag{A25}$$

$$\Delta_\Psi(\tau) = \Delta_\Psi^*(\tau) + \delta\Delta_\Psi(\tau). \tag{A26}$$

Substituting Eqs. (A24)–(A26) into Eqs. (34)–(36) and retaining only linear terms yields the following linear time-dependent differential equation system

$$\boldsymbol{\delta}'(\tau) = J(\tau)\,\boldsymbol{\delta}(\tau), \tag{A27}$$

with $\boldsymbol{\delta} = [\delta A_x(\tau), \delta A_y(\tau), \delta\Delta_\Psi(\tau)]'$ and

$$J(\tau) = \begin{pmatrix} 0 & 0 & 0 \\ 0 & \frac{C A_0^2}{4}\sin\Big(2\Delta_\Psi(\tau)\Big) & 0 \\ A_0\Big(-\frac{3}{4} + C\Big(1 + \frac{1}{2}\cos\big(2\Delta_\Psi(\tau)\big)\Big)\Big) & 0 & -\frac{C A_0^2}{2}\sin\Big(2\Delta_\Psi(\tau)\Big) \end{pmatrix}. \tag{A28}$$

Appendix A.3 Oscillations along the coordinate axes

Eqs. (34)–(36) can be solved in the special case when the oscillations happen along one of the axes. Without loss of generality, let $A_y = 0$. Then, the solution is

In what follows, we restrict ourselves to the solution over one period (i.e., the Floquet multipliers), which determines stability. A positive (real) exponent would indicate instability; marginal stability is achieved when the exponent vanishes, while asymptotic stability is guaranteed for a negative exponent.

We use the phase function given in Eq. (A22) and introduce the abbreviations

$$\alpha(\tau) = \frac{CA_0^2}{4}\,\sin\Big(2\Delta_\Psi^*(\tau)\Big),$$
$$\gamma(\tau) = -\frac{CA_0^2}{2}\,\sin\Big(2\Delta_\Psi^*(\tau)\Big), \tag{A29}$$
$$\beta(\tau) = A_0\Big[-\frac{3}{4} + C\Big(1 + \frac{1}{2}\cos\big(2\Delta_\Psi^*(\tau)\big)\Big)\Big]. \tag{A30}$$

The function $2\Delta_\Psi^*(\tau)$ is odd. Consequently, $\sin\big(2\Delta_\Psi^*(\tau)\big)$ is odd and both $\alpha(\tau)$ and $\gamma(\tau)$ are odd, whereas $\beta(\tau)$ is even.

Magnus expansion over one period

Since $J(t)$ does not commute with its integral $\int_0^t J(s)\mathrm{d}s$, the Magnus expansion has to be used to force the solution into an exponential form. The solution of Eq. (A27) may be written as

$$\boldsymbol{\delta}(\tau) = \exp\Big\{\Omega(\tau, 0)\Big\}\boldsymbol{\delta}(0), \tag{A31}$$

with the Magnus series

$$\Omega(\tau, 0) = \sum_{k\geq 1}\Omega_k(\tau, 0). \tag{A32}$$

In particular, the first two terms are

$$\Omega_1(\tau, 0) = \int_0^\tau J(s)\,\mathrm{d}s, \tag{A33}$$
$$\Omega_2(\tau, 0) = -\frac{1}{2}\int_0^\tau \mathrm{d}s_1 \int_0^{s_1} \mathrm{d}s_2\,[J(s_1), J(s_2)]. \tag{A34}$$

We now set $\tau = T$, where the period is determined by the oscillatory part in Eq. (A22). In fact, define

$$k := \frac{A_0^2\sqrt{3(4C^2 - 8C + 3)}}{8}, \qquad T = \frac{\pi}{k}. \tag{A35}$$

Because $\alpha(\tau)$ and $\gamma(\tau)$ are odd, one immediately has

$$\int_0^T \alpha(\tau)\mathrm{d}\tau = \int_0^T \gamma(\tau)\mathrm{d}\tau = 0. \tag{A36}$$

Thus, the first Magnus term becomes

$$\Omega_1(T, 0) = \begin{pmatrix} 0 & 0 & 0 \\ 0 & 0 & 0 \\ I_\beta & 0 & 0 \end{pmatrix}, \qquad I_\beta = \int_0^T \beta(\tau)\mathrm{d}\tau. \tag{A37}$$

The second Magnus term involves the commutator

$$[J(s_1), J(s_2)] = \begin{pmatrix} 0 & 0 & 0 \\ 0 & 0 & 0 \\ \gamma(s_1)\beta(s_2) - \gamma(s_2)\beta(s_1) & 0 & 0 \end{pmatrix}. \tag{A38}$$

Since $\gamma(s)$ is odd and $\beta(s)$ is even, the integrand

$$k(s_1, s_2) = \gamma(s_1)\beta(s_2) - \gamma(s_2)\beta(s_1) \tag{A39}$$

is antisymmetric over the symmetrized integration domain. Therefore, one obtains

$$\Omega_2(T, 0) = 0. \tag{A40}$$

A similar symmetry argument shows that all higher-order Magnus terms ($\Omega_k(T, 0)$ for $k \geq 3$) vanish as well. Hence, the Magnus expansion truncates after the first term:

$$\Omega(T, 0) = \Omega_1(T, 0) = \begin{pmatrix} 0 & 0 & 0 \\ 0 & 0 & 0 \\ I_\beta & 0 & 0 \end{pmatrix}. \tag{A41}$$

Since $\Omega(T, 0)^2 = 0$, the exponential simplifies to

$$\exp\{\Omega(T, 0)\} = I + \Omega(T, 0) = \begin{pmatrix} 1 & 0 & 0 \\ 0 & 1 & 0 \\ I_\beta & 0 & 1 \end{pmatrix}. \tag{A42}$$

Evaluation of I_β

We now evaluate

$$I_\beta = A_0\int_0^T\Big[-\frac{3}{4} + C\Big(1 + \frac{1}{2}\cos\big(2\Delta_\Psi^*(\tau)\big)\Big)\Big]\mathrm{d}\tau. \tag{A43}$$

Splitting the integral, we write

$$I_\beta = A_0\left\{\Big[-\frac{3}{4} + C\Big]T + \frac{C}{2}\int_0^T \cos\big(2\Delta_\Psi^*(\tau)\big)\mathrm{d}\tau\right\}. \tag{A44}$$

To evaluate the cosine integral, we first express

$$2\Delta_\Psi^*(\tau) = -2\arctan\Big[\sqrt{\frac{6C-3}{2C-3}}\,\tan\Big(k\tau\Big)\Big], \tag{A45}$$

so that (since cosine is even)

$$\cos\big(2\Delta_\Psi^*(\tau)\big) = \cos\Big(2\arctan\Big[\sqrt{\frac{6C-3}{2C-3}}\,\tan\Big(k\tau\Big)\Big]\Big). \tag{A46}$$

Defining

$$D := \sqrt{\frac{6C-3}{2C-3}}, \tag{A47}$$

we use the double-angle formula for the arctan to obtain

$$\cos\big(2\Delta_\Psi^*(\tau)\big) = \frac{1 - D^2\tan^2(k\tau)}{1 + D^2\tan^2(k\tau)}. \tag{A48}$$

Changing variables via $x = k\tau$ (so that $\mathrm{d}\tau = \frac{\mathrm{d}x}{k}$ and the integration limits become 0 to π since $T = \pi/k$), we have

$$\int_0^T \cos\big(2\Delta_\Psi^*(\tau)\big)\mathrm{d}\tau = \frac{1}{k}\int_0^\pi \frac{1 - D^2\tan^2 x}{1 + D^2\tan^2 x}\mathrm{d}x. \tag{A49}$$

By symmetry the integral over $[0, \pi]$ equals twice the integral from 0 to $\pi/2$:

$$\int_0^T \cos\big(2\Delta_\Psi^*(\tau)\big)\mathrm{d}\tau = \frac{2}{k}\int_0^{\pi/2} \frac{1 - D^2\tan^2 x}{1 + D^2\tan^2 x}\mathrm{d}x. \tag{A50}$$

Next, setting $t = \tan x$ (so that $\mathrm{d}x = \frac{\mathrm{d}t}{1+t^2}$ and $x : 0 \to \pi/2$ corresponds to $t : 0 \to \infty$), we obtain

$$\int_0^T \cos\big(2\Delta_\Psi^*(\tau)\big)\mathrm{d}\tau = \frac{2}{k}\int_0^\infty \frac{1 - D^2t^2}{(1+t^2)(1+D^2t^2)}\mathrm{d}t. \tag{A51}$$

A partial-fractions decomposition yields

$$\frac{1 - D^2t^2}{(1+t^2)(1+D^2t^2)} = -\frac{D^2+1}{D^2-1}\frac{1}{1+t^2} + \frac{2D^2}{D^2-1}\frac{1}{1+D^2t^2}. \tag{A52}$$

Since

$$\int_0^\infty \frac{\mathrm{d}t}{1+t^2} = \frac{\pi}{2} \quad \text{and} \quad \int_0^\infty \frac{\mathrm{d}t}{1+D^2t^2} = \frac{\pi}{2D}, \tag{A53}$$

we find that

$$\int_0^\infty \frac{1 - D^2t^2}{(1+t^2)(1+D^2t^2)}\mathrm{d}t = \frac{\pi}{2}\left[-\frac{D^2+1}{D^2-1} + \frac{2D}{D^2-1}\right] = -\frac{\pi}{2}\frac{D-1}{D+1}. \tag{A54}$$

Thus,

$$\int_0^T \cos\big(2\Delta_\Psi^*(\tau)\big)\mathrm{d}\tau = -\frac{\pi}{k}\frac{D-1}{D+1} = -T\,\frac{D-1}{D+1}. \tag{A55}$$

Inserting this into Eq. (A43) we obtain

$$I_\beta = A_0\,T\left[-\frac{3}{4} + C - \frac{C}{2}\frac{D-1}{D+1}\right]. \tag{A56}$$

A straightforward (albeit somewhat lengthy) algebraic manipulation shows that

$$-\frac{3}{4} + C - \frac{C}{2}\frac{D-1}{D+1} = -\frac{1}{4}\sqrt{3(4C^2 - 8C + 3)}. \tag{A57}$$

Thus, we arrive at

$$I_\beta = -\frac{A_0\,T}{4}\sqrt{3(4C^2 - 8C + 3)}. \tag{A58}$$

Recalling Eq. (A35), i.e.

$$T = \frac{8\pi}{A_0^2\sqrt{3(4C^2 - 8C + 3)}}, \tag{A59}$$

we deduce that

$$I_\beta = -\frac{A_0}{4}\frac{8\pi}{A_0^2\sqrt{3(4C^2 - 8C + 3)}}\sqrt{3(4C^2 - 8C + 3)} = -\frac{2\pi}{A_0}. \tag{A60}$$

In particular, the result is independent of C and depends solely on A_0.

Since the Magnus expansion truncates at first order, the one-period solution operator (or Floquet multiplier) is

$$\Phi(T, 0) = \exp\{\Omega(T, 0)\} = I + \Omega(T, 0) = \begin{pmatrix} 1 & 0 & 0 \\ 0 & 1 & 0 \\ -\frac{2\pi}{A_0} & 0 & 1 \end{pmatrix}, \tag{A61}$$

which leads to

$$\delta A_x(T) = \delta A_x(0), \tag{A62}$$

$$\delta A_y(T) = \delta A_y(0), \tag{A63}$$

$$\delta\Delta_\Psi(T) = -\frac{2\pi}{A_0}\delta A_x(0) + \delta\Delta_\Psi(0), \tag{A64}$$

which implies a constant shift of Δ_Ψ in each period, proportional to the relative perturbation of the oscillation amplitude. This is to be expected, as a larger-amplitude oscillation in a degressive potential has a longer time period. Thus, the phase shift increases over time. Although stability in the sense of Lyapunov is not given, the system is orbitally stable, as, by an adequate stretching of time, the perturbed solution can be brought into the infinitesimal vicinity of the unperturbed solution.

Acknowledgements The authors thank Dhruv Singhal for his linguistic suggestions and acknowledge the use of ChatGPT, Grammarly, and Writefull.

Author Contributions A.G. carried out the research and wrote the manuscript. O.G. and A.F. revised the manuscript.

Funding Open Access funding enabled and organized by Projekt DEAL. This research was funded by the Deutsche Forschungsgemeinschaft (DFG, German Research Foundation) under Project Number 508244284. We are sincerely grateful for their support.

Data Availability No datasets were generated or analysed during the current study.

Declarations

Conflicts of Interest The authors have no relevant financial or non-financial interests to disclose.

References

1. Ibrahim, H., Lefebvre, C., Bandrauk, A.D., Staudte, A., Légaré, F.: H_2: The benchmark molecule for ultrafast science and technologies. J. Phys. B: Atomic, Molec. Optic Phys. 51, 042002 (2022)
2. Suzuki, H., Shimakawa, H., Kumada, A., Sato, M.: Molecular dynamics study of ionic conduction in epoxy Resin. IEEE Trans. Dielectr. Electr. Insul. **29**(1), 170–177 (2022). https://doi.org/10.1109/TDEI.2022.3148462
3. Koon, W.S., Lo, M.W., Marsden, J.E., Ross, S.D.: Heteroclinic connections between periodic orbits and resonance transitions in celestial mechanics. Chaos Interdiscip. J. Nonlinear Sci. **10**, 427 (2000)
4. Arnold, V.I., Kozlov, V.V., Neishtadt, A.I.: Mathematical Aspects of Classical and Celestial Mechanics. Springer, Berlin (2006)
5. Cao, J., Zhou, S., Wang, W., Lin, J.: Influence of potential well depth on nonlinear tristable energy harvesting. Appl. Phys. Lett. **106**, 173903 (2015)
6. Barone, A., Paterno, G.: Physics and Applications of the Josephson Effect. Wiley, New York (1982)
7. Maki, A., Miino, Y., Umeda, N., Sakai, M., Ueta, T., Kawakami, H.: Nonlinear dynamics of ship capsizing at sea. Nonlinear Theory and Its Applications, IEICE **13**(1), 2–24 (2022). https://doi.org/10.1587/nolta.13.2
8. Naik, S., Ross, S.D.: Geometry of escaping dynamics in nonlinear ship motion. Commun. Nonlinear Sci. Numer. Simul. **47**, 48–70 (2017)
9. Genda, A., Fidlin, A., Lenci, S., Gendelman, O.: Effects of seasonal hunting and food quantity variations on the lotka-volterra model. Nonlinear Dyn. (2024). https://doi.org/10.1007/s11071-024-10667-y
10. Zhang, W., Yan, H., Peng, Z.K., Meng, G.: Electrostatic pull-in instability in MEMS/NEMS: a review. Sens. Actuators, A **214**, 187–218 (2018)
11. Younis, M.I., Abdel-Rahman, E.M., Nayfeh, A.: A reduced-order model for electrically actuated microbeam-based MEMS. J. Microelectromech. Syst. **12**, 672–680 (2003)
12. Shang, H.: Pull-in instability of a typical electrostatic MEMS resonator and its control by delayed feedback. Nonlinear Dyn. **90**(1), 171–183 (2017)
13. Virgin, L.N.: Approximate criterion for capsize based on deterministic dynamics. Dyn. Stab. Syst. **4**, 56–70 (1989)
14. Virgin, L.N., Plaut, R.H., Cheng, C.-C.: Prediction of escape from a potential well under harmonic excitation. Int. J. Non-Linear Mech. **27**(3), 357–365 (1992). https://doi.org/10.1016/0020-7462(92)90005-R
15. Mann, B.P.: Energy criterion for potential well escapes in a bistable magnetic pendulum. J. Sound Vib. **323**, 864–876 (2009)
16. Gendelman, O.V.: Escape of a harmonically forced classical particle from a potential well: a transient resonance. Nonlinear Dyn. **93**(1), 79–88 (2018)
17. Gendelman, O.V., Karmi, G.: Basic mechanisms of escape of a harmonically forced classical particle from a potential well. Nonlinear Dyn. **98**(4), 2775–2792 (2019)
18. Genda, A., Fidlin, A., Gendelman, O.: On the escape of a resonantly excited couple of colliding particles from a potential well under bi-harmonic excitation. In: European Nonlinear Dynamics Conferences, ENOC, Lyon, sciencesconf (2022)
19. Genda, A., Fidlin, A., Gendelman, O.: The level-crossing problem of a weakly damped particle in quadratic potential well under harmonic excitation. Nonlinear Dynamics 111, 20563–20578 (2023) https://doi.org/10.1007/s11071-023-08875-z
20. Genda, A., Fidlin, A., Gendelman, O.: Dynamics of forced escape from asymmetric truncated parabolic well. ZAMM - Journal of Applied Mathematics and Mechanics / Zeitschrift für Angewandte Mathematik und Mechanik (2023). https://doi.org/10.1002/zamm.202200567
21. Thompson, J.M.T.: Chaotic phenomena triggering the escape from a potential well. Proceedings of the Royal Society of London A **421**, 195–225 (1989)
22. Farid, M., Gendelman, O.V.: Escape of a forced-damped particle from weakly nonlinear truncated potential well. Nonlinear Dyn. **103**, 63–78 (2020)
23. Genda, A., Fidlin, A., Gendelman, O.: On the escape of a resonantly excited couple of particles from a potential well. Nonlinear Dyn. **104**(1), 91–102 (2021)
24. Genda, A., Fidlin, A., Gendelman, O.: Model reduction for an internally damped n-particle chain in a potential well under polyharmonic excitation. Acta Mech. (2024). https://doi.org/10.1007/s00707-024-03972-5
25. Chacón, R., Martínez, P.J., Marcos, J.M., Aranda, F.J.: Ratchet universality in the bidirectional escape from a symmetric potential well. Phys. Rev. E **103**, 022030 (2013)
26. Nieto, A.R., Seoane, J.M., Sanjuán, M.A.F.: Noise activates escapes in closed Hamiltonian systems. Commun. Nonlinear Sci. Numer. Simul. **105**, 106074 (2022)
27. Nieto, A.R., Seoane, J.M., Sanjuán, M.A.F.: Final state sensitivity in noisy chaotic scattering. Chaos, Solitons Fractals **150**, 111168 (2021)
28. Seoane, J.M., Sanjuán, M.A.F.: New developments in classical chaotic scattering. Rep. Prog. Phys. **76**(1), 016001 (2013). https://doi.org/10.1088/0034-4885/76/1/016001. 2013 IOP Publishing Ltd

29. Contopoulos, G., Kandrup, H.E., Kaufmann, D.: Fractal properties of escape from a two-dimensional potential. Physica D **64**, 310–323 (2013)
30. Nayeem, R., Bazzi, S., Sadeghi, M., Hogan, N., Sternad, D.: Preparing to move: Setting initial conditions to simplify interactions with complex objects. PLoS Comput. Biol. **17**(12), 1009597 (2021). https://doi.org/10.1371/journal.pcbi.1009597
31. Zotos, E.E., Jung, C.: A three-dimensional dynamical model for double-barred galaxies, escape dynamics and the role of the nhims. Communications in Nonlinear Science and Numerical Simulation 80, 104989 (2020) https://doi.org/10.1016/j.cnsns.2019.104989
32. Alhussein, H., Daqaq, M.F.: Potential well escape in a galloping twin-well oscillator. Nonlinear Dyn 99, 57–72 (2020) https://doi.org/10.1007/s11071-019-05306-w . Published: 02 November 2019, Issue Date: January 2020
33. Sanjuan, M.A.F.: The effect of nonlinear damping on the universal escape oscillator. Int. J. Bifurc. Chaos **9**, 735–744 (1999)
34. Lenci, S., Benedetti, K.C.B., Rega, G., Gonçalves, P.B.: Stochastic basins of attraction for uncertain initial conditions. Journal of Sound and Vibration 587, 118488 (2024) https://doi.org/10.1016/j.jsv.2024.118488
35. Belardinelli, P., Lenci, S.: Improving the global analysis of mechanical systems via parallel computation of basins of attraction. Procedia IUTAM 22, 192–199 (2017) https://doi.org/10.1016/j.piutam.2017.08.028 . IUTAM Symposium on Nonlinear and Delayed Dynamics of Mechatronic Systems
36. Rega, G., Lenci, S.: Identifying, evaluating, and controlling dynamical integrity measures in non-linear mechanical oscillators. Nonlinear Analysis: Theory, Methods & Applications **63**(5), 902–914 (2005). https://doi.org/10.1016/j.na.2005.01.084
37. Habib, G.: Dynamical integrity assessment of stable equilibria: a new rapid iterative procedure. Nonlinear Dyn. **106**(3), 2073–2096 (2021). https://doi.org/10.1007/s11071-021-06936-9
38. Belardinelli, P., Lenci, S., Rega, G.: Seamless variation of isometric and anisometric dynamical integrity measures in basins's erosion. Communications in Nonlinear Science and Numerical Simulation 56, 499–507 (2018) https://doi.org/10.1016/j.cnsns.2017.08.030
39. Kravetc, P., Gendelman, O., Fidlin, A.: Dynamical integrity of the safe basins in a problem of forced escape. Chaos: An Interdisciplinary Journal of Nonlinear Science 34(8), 083118 (2024) https://doi.org/10.1063/5.0205049
40. Karmi, G., Kravetc, P., Gendelman, O.: Analytic exploration of safe basins in a benchmark problem of forced escape. Nonlinear Dynamics 106, 1573–1589 (2021) https://doi.org/10.1007/s11071-021-06942-x
41. Engel, A., Gendelman, O.V., Fidlin, A.: Escape of a particle from two-dimensional potential well. Nonlinear Dyn. (2023). https://doi.org/10.1007/s11071-023-09154-7
42. Gendelman, O.V., Sapsis, T.P.: Energy exchange and localization in essentially nonlinear oscillatory systems: Canonical formalism. J. Appl. Mech. **84**(1), 011009 (2016). https://doi.org/10.1115/1.4034930
43. Gilchrist, A.O.: The free oscillations of conservative quasilinear systems with two degrees of freedom. Int. J. Mech. Sci. **3**(4), 286–311 (1961). https://doi.org/10.1016/0020-7403(61)90027-3
44. Kronauer, R.E., Musa, S.A.: Exchange of energy between oscillations in weakly nonlinear conservative systems. J. Appl. Mech. **33**, 451–452 (1966)
45. Musa, S.A.: Integral constraints in weakly nonlinear periodic systems. SIAM J. Appl. Math. **15**(5), 1324–1327 (1967). https://doi.org/10.1137/0115115
46. Augusteijn, M.F., Breitenberger, E.: Integration of near-resonant systems in slow-fluctuation approximation. J. Math. Phys. **21**, 462–471 (1980)
47. Breitenberger, E., Mueller, R.D.: The elastic pendulum: A nonlinear paradigm. J. Math. Phys. **22**, 1196–1210 (1981)
48. Bogoliubov, N.N., Mitropolskii, Y.A.: Asymptotic Methods in the Theory of Non-Linear Oscillations. Gordon & Breach Science Publishers, New York (1961). Translated from the Russian original (Nauka, Moscow, 1959) on the Krylov–Bogolyubov-Mitropolskii averaging method
49. *NIST Digital Library of Mathematical Functions*. https://dlmf.nist.gov/, Release 1.2.4 of 2025-03-15. F. W. J. Olver, A. B. Olde Daalhuis, D. W. Lozier, B. I. Schneider, R. F. Boisvert, C. W. Clark, B. R. Miller, B. V. Saunders, H. S. Cohl, and M. A. McClain, eds.
50. Efron, B.: Bootstrap methods: Another look at the jackknife. Ann. Stat. **7**(1), 1–26 (1979). https://doi.org/10.1214/aos/1176344552